Symplectic Hamiltonian finite element methods for electromagnetics

Manuel A. Sánchez[1]

Institute for Mathematical and Computational Engineering, School of Engineering and Faculty of Mathematics, Pontificia Universidad Católica de Chile, Santiago, Chile

Shukai Du

Department of Mathematics, University of Wisconsin-Madison, WI 53706, USA

Bernardo Cockburn[2]

School of mathematics, University of Minnesota, Minneapolis, MN 55455, USA

Ngoc-Cuong Nguyen

Department of Aeronautics and Astronautics, Massachusetts Institute of Technology, Cambridge, MA 02139, USA

Jaime Peraire

Department of Aeronautics and Astronautics, Massachusetts Institute of Technology, Cambridge, MA 02139, USA

Abstract

We present a general approach for devising high-order accurate finite element methods for the Maxwell's equations based on two different Hamiltonian structures of the Maxwell's equations, namely, the standard formulation of the equations in terms of the electric and magnetic fields, and a wave-like rewriting of the standard formulation in terms of the electric and the magnetic potential fields. For each of these Hamiltonian structures, we introduce spatial discretizations of the Maxwell's equations using mixed finite element, discontinuous Galerkin, and hybridizable discontinuous Galerkin methods to obtain a semi-discrete system of equations which inherit the Hamiltonian structure of the Maxwell's equations. We discretize the resulting semi-discrete system in time by using a symplectic integrator to ensure the conservation properties of the fully discrete system of equations. We show that the methods provide time-invariant, non-drifting

Email addresses: manuel.sanchez@uc.cl (Manuel A. Sánchez), shukaidu@udel.edu (Shukai Du), cockburn@math.umn.edu (Bernardo Cockburn), cuongng@mit.edu (Ngoc-Cuong Nguyen), peraire@mit.edu (Jaime Peraire)

[1]M. A. Sánchez was partially supported by FONDECYT Iniciación n.11180284 grant
[2]B. Cockburn was partially supported by NSF via DMS-1912646 grant.

approximations of the total electric, magnetic charges, and the total energy. There is a Symplectic DG method for the first formulation [J. Sci. Comput. 35, pp. 241–265, 2008] but all other methods are new. We show that there are no Symplectic HDG methods for the first formulation. In contrast, we devise Symplectic Hamiltonian mixed, DG, and HDG methods for the second formulation. For the Symplectic HDG method, we present numerical experiments which confirm its optimal orders of convergence for all variables and its conservation properties for the total linear and angular momenta, the electric and magnetic charges, as well as the total energy. Finally, we discuss the extension of our results to other boundary conditions and to numerical schemes defined by different weak formulations.

Keywords: time-dependent Maxwell's equations, symplectic Hamiltonian finite element methods, mixed methods, discontinuous Gakerkin methods, hybridizable discontinuous Galerkin methods.
2010 MSC: 65M60, 74H15, 74J05, 74S05

---

1. Introduction

This paper is part of a series [56, 57] devoted to the development of what can be called the Symplectic Hamiltonian (SH) finite element methods. These methods are developed for time-dependent partial differential equations (PDEs) with Hamiltonian structure. To obtain the methods, we first discretize the governing equations in space by using a finite element method which is devised to produce a system of ordinary differential equations (ODEs) with Hamiltonian structure. Then, we apply a symplectic, time-marching scheme to the system of ODEs in order to ensure that the discrete Hamiltonian (the discrete energy) is either perfectly conserved or does not drift in time. Arbitrary high-order accuracy in both time and space can be achieved by these methods.

Several symplectic Hamiltonian finite element methods were introduced in [56] for the acoustic wave equation, and in [57] for the equations of linear elastodynamics. In particular, we devised the first hybridizable discontinuous Galerkin (HDG) methods for the acoustic wave equation to display a constant or non-drifting discrete energy [56]. In [57], we obtained the first HDG methods for linear elastodynamics that conserve both the global linear and angular momentum *and* display a constant or non-drifting discrete energy.

In this paper, we continue this effort and develop SH finite element methods for the Maxwell's equations in a polyhedral domain Ω:

$$
\begin{aligned}
\epsilon\,\dot{\boldsymbol{E}} &= \nabla\times\boldsymbol{H}-\boldsymbol{J} && \text{in } \Omega\times(0,T], && \text{(1a)}\\
\mu\,\dot{\boldsymbol{H}} &= -\nabla\times\boldsymbol{E} && \text{in } \Omega\times(0,T], && \text{(1b)}\\
\nabla\cdot(\epsilon\,\boldsymbol{E}) &= \rho && \text{in } \Omega\times(0,T], && \text{(1c)}\\
\nabla\cdot(\mu\,\boldsymbol{H}) &= 0 && \text{in } \Omega\times(0,T], && \text{(1d)}
\end{aligned}
$$

with the following boundary and initial conditions:

$$\boldsymbol{n} \times \boldsymbol{E} = \boldsymbol{g}_{\boldsymbol{E}} \qquad \text{on } \Gamma \times (0, T], \qquad \Gamma := \partial\Omega, \tag{1e}$$

$$\boldsymbol{E} = \boldsymbol{E}_0, \ \boldsymbol{H} = \boldsymbol{H}_0 \qquad \text{on } \Omega \times \{t = 0\}. \tag{1f}$$

Here, $\boldsymbol{E}$ and $\boldsymbol{H}$ are the electric and magnetic fields, respectively; ρ and $\boldsymbol{J}$ represent the scalar charge density function and the vector current density function, respectively; and ϵ and μ, the electric permitivitty and magnetic permeability, respectively, which we assume are positive functions independent of time. The speed of light is $c := 1/\sqrt{\epsilon\mu}$. Other electromagnetic quantities of interest are described in Table 1.

Table 1: Glosary of electromagnetic quantities.

name	symbol	definition
energy	$\mathcal{E}$	$\frac{1}{2}(\epsilon \boldsymbol{E} \cdot \boldsymbol{E} + \mu \boldsymbol{H} \cdot \boldsymbol{H})$
energy flux, Poynting vector	$\boldsymbol{S}$	$\boldsymbol{E} \times \boldsymbol{H}$
linear momentum	$\boldsymbol{P}$	$\epsilon\, \boldsymbol{E} \times \mu \boldsymbol{H}$
Lorentz force	$\boldsymbol{F}$	$\rho\, \boldsymbol{E} + \boldsymbol{J} \times \mu \boldsymbol{H}$
angular momentum	$\boldsymbol{L}$	$\boldsymbol{x} \times \boldsymbol{P}$
Maxwell's stress	$\underline{\boldsymbol{\sigma}}$	$-\mathcal{E}\, \underline{\boldsymbol{I}} + \epsilon\, \boldsymbol{E} \otimes \boldsymbol{E} + \mu \boldsymbol{H} \otimes \boldsymbol{H}$
quantities associated to the Lipkin's zilch tensor		
optical chirality [62]	χ	$\frac{1}{2}(\epsilon\, \boldsymbol{E} \cdot \nabla \times \boldsymbol{E} + \mu \boldsymbol{H} \cdot \nabla \times \boldsymbol{H})$
optical chirality flux	$\boldsymbol{X}$	$\frac{1}{2}(\boldsymbol{E} \times (\nabla \times \boldsymbol{H}) + (\nabla \times \boldsymbol{E}) \times \boldsymbol{H})$
flux of the optical chirality flux	$\underline{\boldsymbol{X}}$	$\chi\, \underline{\boldsymbol{I}} - \frac{1}{2}(\frac{1}{\mu} \boldsymbol{E} \otimes (\nabla \times \boldsymbol{E}) + \frac{1}{\epsilon} \boldsymbol{H} \otimes (\nabla \times \boldsymbol{H}) + (\nabla \times \boldsymbol{E}) \otimes \frac{1}{\mu} \boldsymbol{E} + (\nabla \times \boldsymbol{H}) \otimes \frac{1}{\epsilon} \boldsymbol{H})$

The SH finite element methods devised herein are of arbitrary order of accuracy and are able to approximate well the integral over Ω of each of the quantities in the rich set of conservation laws of the Maxwell's equations listed on Table 2. As we can see in Table 2, there are conservation laws for the linear functional of total magnetic charge and of total electric charge, as well as for the quadratic functional of the total electromagnetic energy, the total linear and angular electromagnetic momenta, the total optical chirality[3], its flux and of the flux of its flux. The conservation laws for these optical chirality quantities are related to the conservation laws found by Lipkin back in 64 [38]; see also how optical chirality quantities are related to Lipkin's rank-three <u>zilch</u> tensor, [9, equation(8.1)]. We prove that discrete version of the magnetic and electric charges, and of the energy remain exactly constant or do not drift in time. To the best knowledge of the authors, none of these properties holds for any DG

[3]Not to be confused with the electromagnetic helicity which was defined back in 83 [1] as c^2 times the optical chirality χ. For a modern definition of the electromagnetic helicity, see [9] and the references therein.

Table 2: Conservation law for the (scalar or vectorial) electromagnetic quantity η, $\dot{\eta} + \nabla \cdot f_\eta = S_\eta$, deduced from the first two Maxwell's equations. The flux of η is denoted by f_η, and the corresponding sources and sinks, by S_η.

conservation of	η	f_η	S_η
magnetic charge	$\nabla \cdot (\mu \boldsymbol{H})$	$\boldsymbol{0}$	0
electric charge	$\nabla \cdot (\epsilon \boldsymbol{E})$	$\boldsymbol{J}$	0
energy	$\mathcal{E}$	$\boldsymbol{S}$	$-\boldsymbol{E} \cdot \boldsymbol{J}$
linear momentum	$\boldsymbol{P}$	$-\underline{\boldsymbol{\sigma}}$	$-\boldsymbol{F} + \frac{1}{2}(\boldsymbol{E} \cdot \boldsymbol{E} \nabla \epsilon + \boldsymbol{H} \cdot \boldsymbol{H} \nabla \mu)$
angular momentum	$\boldsymbol{L}$	$-\boldsymbol{x} \times \underline{\boldsymbol{\sigma}}$	$\boldsymbol{x} \times \boldsymbol{S}_{\boldsymbol{P}}$
for $\rho = 0, \boldsymbol{J} = \boldsymbol{0}$ and homogeneous media			
optical chirality	χ	$\boldsymbol{X}$	0
optical chirality flux	$\boldsymbol{X}$	$\underline{\boldsymbol{X}}$	0
flux of the ij-th entry of the optical chirality flux	$\underline{\boldsymbol{X}}_{ij}$	$c^2 \, \delta_{ij} \, \boldsymbol{X} + \frac{c^2}{2}(-\boldsymbol{E}_i \nabla \boldsymbol{H}_j + \boldsymbol{H}_j \nabla \boldsymbol{E}_i - \boldsymbol{E}_j \nabla \boldsymbol{H}_i + \boldsymbol{H}_i \nabla \boldsymbol{E}_j)$	0

[24, 47, 30, 20, 29, 13] or HDG [15] method for the time-dependent Maxwell's equations in three space dimensions. Moreover, our numerical results show that the conservation laws for the linear and angular momenta are extremely well approximated.

The schemes developed here are certainly not the first to be able to maintain a constant discrete total electromagnetic energy. Examples of energy-conserving numerical schemes are the popular finite-difference Yee's scheme, obtained back in the mid 60's [64], and the splitting finite-difference schemes proposed in [14]. However, the SH finite element methods maintain a discrete version of the Hamiltonian structure of the original partial differential equations, which can be exploited to systematically study the approximation of the functionals displayed on Table 2.

The use of symplectic time-marching methods for integrating Hamiltonian ordinary differential equations has a long history [41, 7]. For Maxwell's equations, SH schemes using finite-difference or finite-volume for the space discretization have been developed, for example, in [32, 61]. However, the schemes presented here are the first SH methods to use mixed, DG or HDG methods for the Maxwell's equations.

In the recent work [26], where new DG discretizations to linear, symmetric hyperbolic systems (like the Maxwell's equations) are introduced which conserve exactly the energy. These methods rely on high-order accurate energy-conserving time-marching methods whereas our methods rely on symplectic methods. Also, the methods in [26] have to use twice as many variables as our methods. On the other hand, our methods can only be applied to equations with Hamiltonian structure, whereas the methods in [26] can be applied to any linear, symmetric hyperbolic system.

The SH finite element schemes are devised in two ways. Each way is associated with a different Hamiltonian structure of the Maxwell's equations. The first is associated with the original form of the equations (1), which we call the $\boldsymbol{E}$-$\boldsymbol{H}$ formulation. It is well known that the standard DG methods for this formulation [21, 24, 22, 30, 47, 20, 29, 13] do not make use of the Hamiltonian structure of the equations. Instead, they use the fact that the equations constitute a symmetric, hyperbolic system. This results, in a natural way, in dissipative methods which do not conserve the total energy. In this paper, we show how to take advantage of the Hamiltonian structure of the original Maxwell's equations to obtain SH finite element methods. We show that such methods can be obtained when a mixed method is used, or when a DG method using alternating fluxes, as show in [63] for the 2D Maxwell's equations and other Hamiltonians systems. However, it is not possible to obtain Symplectic HDG methods for this formulation. This motivates the second way of devising SH finite element schemes.

The second is associated to a rewriting of the $\boldsymbol{E}$-$\boldsymbol{H}$ formulation, which we call the $\boldsymbol{E}$-$\boldsymbol{A}$ formulation, namely,

$$\begin{aligned} \dot{\boldsymbol{A}} &= -\boldsymbol{E} && \text{in } \Omega \times (0,T], && \text{(2a)} \\ \epsilon\,\dot{\boldsymbol{E}} &= \nabla \times (\frac{1}{\mu}\nabla \times \boldsymbol{A}) - \boldsymbol{J} && \text{in } \Omega \times (0,T], && \text{(2b)} \\ \nabla \cdot (\epsilon\,\boldsymbol{E}) &= \rho && \text{in } \Omega \times (0,T], && \text{(2c)} \end{aligned}$$

completed with the following boundary and initial conditions:

$$\begin{aligned} &\boldsymbol{n} \times \boldsymbol{A} = \boldsymbol{g}_{\boldsymbol{A}} && \text{on } \Gamma \times (0,T], && \text{(2d)} \\ &\boldsymbol{E} = \boldsymbol{E}_0,\ \boldsymbol{A} = \boldsymbol{A}_0 && \text{on } \Omega \times \{t = 0\}. && \text{(2e)} \end{aligned}$$

where $\boldsymbol{A}$ is a magnetic potential, that is, $\mu\boldsymbol{H} = \nabla \times \boldsymbol{A}$, and $\boldsymbol{g}_{\boldsymbol{A}}(t) := -\int_0^t \boldsymbol{g}_{\boldsymbol{E}}$. The above system has a different Hamiltonian structure which is associated to a wave equation for $\boldsymbol{A}$, namely,

$$\epsilon\ddot{\boldsymbol{A}} + \nabla \times (\frac{1}{\mu}\nabla \times \boldsymbol{A}) = \boldsymbol{J}.$$

We shall devise a new class of mixed, DG and HDG methods to provide time-invariant non-drifting approximations of the $\boldsymbol{E}$-$\boldsymbol{A}$ formulation.

The remaining of the paper is organized as follows. In Section 2, we discuss in detail the two Hamiltonian structures of the Maxwell's equations. In Section 3, we present the spatial discretization methods and in Section 4, we prove that they result in a set of ODEs with Hamiltonian structure. We then prove the corresponding conservation laws. In Section 5, for an HDG method for the $\boldsymbol{E} - \boldsymbol{A}$ formulation, we present the corresponding fully discrete SH methods. In Section 6, we explore its convergence and conservation properties. Finally, in Section 7, we discuss the treatment of other boundary conditions, and how to devise methods for different weak formulations.

2. The Hamiltonian structure of Maxwell's equations

In this Section, we show that the Maxwell's equations (1) and (2) are Hamiltonian. A dynamical system is Hamiltonian if it can be written as

$$\dot{F} \;=\; \{F,\, \mathcal{H}\},$$

where F are the coordinate functionals, which can be identified to the space of test functions $\mathcal{D}$, $\mathcal{H}$ is the Hamiltonian functional both defined on the phase affine space $\mathcal{M}$, and $\{\cdot,\cdot\}$ denotes the Poisson bracket [41]. We recall that the Poisson bracket is a bilinear anti-symmetric form which satisfies the Jacobi identity. We then say that $(\mathcal{M}, \{\cdot,\cdot\}, \mathcal{H})$ defines a Hamiltonian dynamical system.

2.1. Notation

We begin by introducing some basic notation. The standard spaces of vector-valued functions we are going to work with are

$$\begin{aligned}\boldsymbol{L}^2(D) :=& \{\boldsymbol{v} : D \longrightarrow \mathbb{R}^3 : \|\boldsymbol{v}\|_{L^2(D)} < \infty\},\\ \mathbf{H}(\mathrm{curl}, \mathrm{D}) :=& \{\boldsymbol{v} \in \boldsymbol{L}^2(D) :\ \nabla \times \boldsymbol{v} \in \boldsymbol{L}^2(D)\}.\end{aligned}$$

For any vector-valued function $\boldsymbol{v}$ defined in the domain Ω, we denote its trace on Γ by $\boldsymbol{v}|_\Gamma$. We denote the exterior trace of $\boldsymbol{v}$ on Γ by $\boldsymbol{v}^{ext}$. The exterior trace is defined independently of the regularity of the function $\boldsymbol{v}$ inside Ω. Moreover, even $\boldsymbol{v}|_\Gamma$ is well defined, it does not have to coincide with the exterior trace $\boldsymbol{v}^{ext}$.

Finally, for any given space $\boldsymbol{S}(\circ)$ of functions defined in the interior of Ω where "$\circ$" represents, for example, "Ω" or "curl, Ω", we set

$$\boldsymbol{S}^{\,\mathrm{trace}}(\circ; \boldsymbol{g}) := \{\boldsymbol{s} \in \boldsymbol{S}(\circ) :\ \boldsymbol{n} \times \boldsymbol{s}^{\mathrm{trace}} = \boldsymbol{g} \text{ on } \Gamma\},$$

where "trace" indicates if the trace is the standard trace or the exterior trace. In the first case, we drop the superscript and in the second case, we write "ext". We use the notion of exterior trace in order to properly establish the Hamiltonian structure of the Maxwell's equations. In particular, the exterior trace allows us to easily incorporate the boundary condition on the electric field into the smooth manifold $\mathcal{M}$.

2.2. Electric and magnetic field formulation.

We assume that ϵ, μ, ρ, $\boldsymbol{J}$ and $\boldsymbol{g_E}$ are independent of time. We also assume that the current $\boldsymbol{J}$ is solenoidal. Thus, we can write that

$$\boldsymbol{J} = \nabla \times \boldsymbol{J}_\times.$$

The components of the Hamiltonian structure are:

(i) The phase manifold and the space of test functions:

$$\mathcal{M} = \boldsymbol{L}^{2,ext}(\Omega; \boldsymbol{g_E}) \times \mathbf{H}(\mathrm{curl}, \Omega), \tag{3a}$$

$$\mathcal{D} = \mathcal{C}^{\infty,ext}(\Omega; \mathbf{0}) \quad \times \mathcal{C}^{\infty}(\Omega). \tag{3b}$$

(ii) The Poisson bracket is

$$
\begin{aligned}
\{F, G\}_{\mathcal{E}} = \; & \int_\Omega \left(\frac{1}{\epsilon} \frac{\delta F}{\delta \boldsymbol{E}} \cdot \nabla \times \left(\frac{1}{\mu} \frac{\delta G}{\delta \boldsymbol{H}} \right) - \left(\frac{1}{\epsilon} \frac{\delta G}{\delta \boldsymbol{E}} \right) \cdot \nabla \times \left(\frac{1}{\mu} \frac{\delta F}{\delta \boldsymbol{H}} \right) \right) \\
& + \int_\Gamma \left(\boldsymbol{n} \times \left(\frac{1}{\epsilon} \frac{\delta F}{\delta \boldsymbol{E}} \right)^{ext} \cdot \left(\frac{1}{\mu} \frac{\delta G}{\delta \boldsymbol{H}} \right) - \boldsymbol{n} \times \left(\frac{1}{\epsilon} \frac{\delta G}{\delta \boldsymbol{E}} \right)^{ext} \cdot \left(\frac{1}{\mu} \frac{\delta F}{\delta \boldsymbol{H}} \right) \right).
\end{aligned}
\tag{3c}
$$

Here $F = F(\boldsymbol{E}, \boldsymbol{H})$ and $G = G(\boldsymbol{E}, \boldsymbol{H})$ are functionals on $\mathcal{M}$ and the operators $\frac{\delta}{\delta \boldsymbol{E}}$, $\frac{\delta}{\delta \boldsymbol{H}}$ are the functional derivatives, that is,

$$
\int_\Omega \frac{\delta F}{\delta \boldsymbol{E}} \cdot \boldsymbol{\phi} = \frac{d}{d\varepsilon} F(\boldsymbol{E} + \varepsilon\, \boldsymbol{\phi}, \boldsymbol{H}), \quad \int_\Omega \frac{\delta F}{\delta \boldsymbol{H}} \cdot \boldsymbol{\psi} = \frac{d}{d\varepsilon} F(\boldsymbol{E}, \boldsymbol{H} + \varepsilon\, \boldsymbol{\psi}).
$$

(iii) The Hamiltonian (the total electromagnetic energy):

$$
\mathcal{H}_{\mathcal{E}}(\boldsymbol{E}, \boldsymbol{H}) \;=\; \frac{1}{2} \int_\Omega (\epsilon\, \boldsymbol{E} \cdot \boldsymbol{E} + \mu\, \boldsymbol{H} \cdot \boldsymbol{H}) - \int_\Omega \boldsymbol{J}_\times \cdot \mu \boldsymbol{H}. \tag{3d}
$$

(iv) The coordinate functionals

$$
F_{\boldsymbol{E}}(\boldsymbol{\phi}) = \int_\Omega \epsilon\, \boldsymbol{E} \cdot \boldsymbol{\phi}, \quad F_{\boldsymbol{H}}(\boldsymbol{\psi}) = \int_\Omega \mu\, \boldsymbol{H} \cdot \boldsymbol{\psi} \qquad \forall (\boldsymbol{\phi}, \boldsymbol{\psi}) \in \mathcal{D}. \tag{3e}
$$

It can be shown that the weak solution of the $\boldsymbol{E}$-$\boldsymbol{A}$ formulation (2) defines a Hamiltonian dynamical system for $(\mathcal{M}, \{\cdot,\cdot\}_w, \mathcal{H}_w)$.

2.3. Electric field and magnetic vector potential formulation.

Since $\mu \boldsymbol{H} = \nabla \times \boldsymbol{A}$, we consider $\boldsymbol{H}$ as a function of $\boldsymbol{A}$ and define it as the element of $\boldsymbol{\mathcal{H}}(\mathrm{curl}, \Omega)$ such that

$$
\int_\Omega \mu\, \boldsymbol{H} \cdot \boldsymbol{\psi} = \int_\Omega \boldsymbol{A} \cdot \nabla \times \boldsymbol{\psi} + \int_\Gamma \boldsymbol{g}_{\boldsymbol{A}} \cdot \boldsymbol{\psi} \qquad \forall\, \boldsymbol{\psi} \in \mathbf{H}(\mathrm{curl}, \Omega).
$$

The components of the Hamiltonian structure are:

(i) The phase manifold and the space of test functions are

$$
\mathcal{M} = \boldsymbol{L}^2(\Omega) \times \boldsymbol{L}^{2,ext}(\Omega; \boldsymbol{g}_{\boldsymbol{A}}), \tag{4a}
$$

$$
\mathcal{D} = \mathcal{C}^\infty(\Omega) \times \mathcal{C}^{\infty,ext}(\Omega; \mathbf{0}), \tag{4b}
$$

(ii) The Poisson bracket

$$
\{F, G\}_w \;=\; \int_\Omega \frac{1}{\epsilon} \left(\frac{\delta G}{\delta \boldsymbol{A}} \cdot \frac{\delta F}{\delta \boldsymbol{E}} - \frac{\delta F}{\delta \boldsymbol{A}} \cdot \frac{\delta G}{\delta \boldsymbol{E}} \right), \tag{4c}
$$

where $F = F(\boldsymbol{E}, \boldsymbol{A})$ and $G = G(\boldsymbol{E}, \boldsymbol{A})$ are functionals on $\mathcal{M}$ and the operators $\frac{\delta}{\delta \boldsymbol{E}}$, $\frac{\delta}{\delta \boldsymbol{A}}$ are the functional derivatives.

(iii) The Hamiltonian

$$\mathcal{H}_w(\boldsymbol{E}, \boldsymbol{A}) \;=\; \frac{1}{2}\int_\Omega \big(\epsilon \boldsymbol{E}\cdot\boldsymbol{E} + \mu \boldsymbol{H}\cdot\boldsymbol{H}\big) - \int_\Omega \boldsymbol{A}\cdot\boldsymbol{J}. \tag{4d}$$

(iv) The coordinate functionals

$$F_{\boldsymbol{E}}(\boldsymbol{\phi}) = \int_\Omega \epsilon \boldsymbol{E}\cdot\boldsymbol{\phi}, \quad F_{\boldsymbol{A}}(\boldsymbol{\varphi}) = \int_\Omega \epsilon \boldsymbol{A}\cdot\boldsymbol{\varphi} \qquad (\phi, \psi) \in \mathcal{D}. \tag{4e}$$

It can be shown that if $(\mathcal{M}, \{\cdot,\cdot\}_{\mathcal{E}}, \mathcal{H}_{\mathcal{E}})$ defines a Hamiltonian dynamical system, then it yields the weak solution of the $\boldsymbol{E}$-$\boldsymbol{A}$ formulation (2).

2.4. Conservation laws

The Hamiltonian systems described earlier satisfy all the conservation laws displayed in Table 2. For instance, let us prove the conservation of electric charge, $\dot{\rho}+\nabla\cdot\boldsymbol{J} = 0$, for the wave-like Hamiltonian system $((\mathcal{M}, \mathcal{T}), \{\cdot,\cdot\}_w, \mathcal{H}_w)$. Taking $C := -\int_\Omega \epsilon \boldsymbol{E}\cdot\nabla\phi$, where $\phi \in C_0^\infty(\Omega)$, we obtain

$$\int_\Omega \dot{\rho}\,\phi = -\int_\Omega \epsilon \dot{\boldsymbol{E}}\cdot\nabla\phi = \dot{C} = \{C, \mathcal{H}_w\}_w = \int_\Omega \boldsymbol{J}\cdot\nabla\phi = -\int_\Omega \nabla\cdot\boldsymbol{J}\phi,$$

which proves the conservation of the electric charge. The rest of the conservation laws in Table 2 can be obtained similarly by choosing different functionals C; see Table 3.

Table 3: Conservation laws and their corresponding functional and Poisson bracket. The test functions $\phi \in C_0^\infty(\Omega)$ and $\boldsymbol{\psi} \in C_0^\infty(\Omega; \mathbb{R}^3)$.

conservation laws	functional C	Poisson bracket $\{C, \mathcal{H}_{\mathcal{E}}\}_{\mathcal{E}}$
magnetic charge	$-\int_\Omega \mu\boldsymbol{H}\cdot\nabla\phi$	0
electric charge	$-\int_\Omega \epsilon\boldsymbol{E}\cdot\nabla\phi$	$-\int_\Omega \nabla\cdot\boldsymbol{J}\phi$
energy	$\int_\Omega \mathcal{E}\phi$	$-\int_\Omega(\nabla\cdot\boldsymbol{S} + \boldsymbol{E}\cdot\boldsymbol{J})\phi$
linear momentum	$\int_\Omega \boldsymbol{P}\cdot\boldsymbol{\psi}$	$\int_\Omega(\nabla\cdot\boldsymbol{\sigma} - \boldsymbol{F} + \frac{1}{2}(\lvert\boldsymbol{E}\rvert^2\nabla\epsilon + \lvert\boldsymbol{H}\rvert^2\nabla\mu))\cdot\boldsymbol{\psi}$
angular momentum	$\int_\Omega \boldsymbol{L}\cdot\boldsymbol{\psi}$	$\int_\Omega(\nabla\cdot(\boldsymbol{x}\times\underline{\boldsymbol{\sigma}}) + \boldsymbol{x}\times\boldsymbol{S}_P)\cdot\boldsymbol{\psi}$
for $\rho = 0$, $\boldsymbol{J} = 0$ and homogeneous media		
optical chirality	$\int_\Omega \chi\phi$	$-\int_\Omega \nabla\cdot\boldsymbol{X}\phi$
optical chirality flux	$\int_\Omega \boldsymbol{X}\cdot\boldsymbol{\psi}$	$-\int_\Omega(\nabla\cdot\underline{\boldsymbol{X}})\cdot\boldsymbol{\psi}$
flux of the ij-th entry of the optical chirality flux	$\int_\Omega \underline{\boldsymbol{X}}_{ij}\phi$	$-\int_\Omega \nabla\cdot\big(c^2\delta_{ij}\boldsymbol{X} + \frac{c^2}{2}(-\boldsymbol{E}_i\nabla\boldsymbol{H}_j + \boldsymbol{H}_j\nabla\boldsymbol{E}_i - \boldsymbol{E}_j\nabla\boldsymbol{H}_i + \boldsymbol{H}_i\nabla\boldsymbol{E}_j)\big)\phi$

3. The finite element methods for space discretization

In this section we present the mixed, DG and HDG methods for the spatial discretization of the $\boldsymbol{E}$-$\boldsymbol{H}$ and $\boldsymbol{E}$-$\boldsymbol{A}$ formulations of Maxwell's equations.

3.1. Notation

Let $\mathcal{T}_h = \{K\}$ be a family of conforming, regular triangulations of $\overline{\Omega}$. Let h_K be the inner diameter of an element K in $\mathcal{T}_h$ and we define by h the maximum over the elements. We define the following sets:

$\partial\mathcal{T}_h$: the set of ∂K for all elements K of the triangulation $\mathcal{T}_h$,

$\mathcal{F}_h$: the set of all the faces of the triangulation $\mathcal{T}_h$,

$\mathcal{F}_h^0$: the set of the interior faces of the triangulation $\mathcal{T}_h$,

$\mathcal{F}_h^\partial$: the set of faces lying on the boundary Γ,

∂K: the set of all the faces of the element K

Similar definitions for the inner products in $(d-1)$-dimensional domains with codimension 1 are considered. For a vector-valued function $\boldsymbol{w}$, we define its tangential and normal component, $\boldsymbol{w}^t$ and $\boldsymbol{w}^n$, respectively, over $F \in \mathcal{F}_h$ with normal vector $\boldsymbol{n}$ by

$$\boldsymbol{w}^t = (\boldsymbol{n} \times \boldsymbol{w}) \times \boldsymbol{n}, \qquad \boldsymbol{w}^n = \boldsymbol{n}(\boldsymbol{n} \cdot \boldsymbol{w}).$$

For $D \subset \mathbb{R}^d$ and $B \subset \mathbb{R}^{d-1}$, we denote by $(\cdot,\cdot)_D$ and $\langle \cdot,\cdot \rangle_B$ the inner products for $\boldsymbol{w}, \boldsymbol{v}$ as

$$(\boldsymbol{w}, \boldsymbol{v})_D = \int_D \boldsymbol{w} \cdot \boldsymbol{v}, \qquad \langle \boldsymbol{w}, \boldsymbol{v} \rangle_D = \int_D \boldsymbol{w} \cdot \boldsymbol{v}.$$

Then, we define the inner products over the triangulation $\mathcal{T}_h$ and the sets of boundary and faces of $\mathcal{T}_h$

$$(\boldsymbol{w}, \boldsymbol{v})_{\mathcal{T}_h} = \sum_{K \in \mathcal{T}_h} (\boldsymbol{w}, \boldsymbol{v})_K \quad \langle \boldsymbol{w}, \boldsymbol{v} \rangle_{\partial\mathcal{T}_h} = \sum_{K \in \mathcal{T}_h} \langle \boldsymbol{w}, \boldsymbol{v} \rangle_{\partial K}, \quad \langle \boldsymbol{w}, \boldsymbol{v} \rangle_{\mathcal{G}} = \sum_{F \in \mathcal{G}} \langle \boldsymbol{w}, \boldsymbol{v} \rangle_F,$$

where $\mathcal{G}$ denotes a collection of faces, for instance $\mathcal{G} = \partial K, \mathcal{F}_h, \mathcal{F}_h^0, \mathcal{F}_h^\partial$.

For an interior face $F \in \mathcal{F}_h^0$, we have two elements K^- and K^+ such that $F = \partial K^+ \cap \partial K^-$, and denoting the trace of a vector valued function $\boldsymbol{w}$ to the boundary of $K^\pm$ by $\boldsymbol{w}^\pm$. Then, we define the average and jump on $F \in \mathcal{F}_h^0$ of $\boldsymbol{w}$ by

$$\{\!\{\boldsymbol{w}\}\!\} := \frac{1}{2}(\boldsymbol{w}^+ + \boldsymbol{w}^-), \quad [\![\boldsymbol{w}]\!] := \boldsymbol{n}^+ \times \boldsymbol{w}^+ + \boldsymbol{n}^- \times \boldsymbol{w}^- \quad \text{for } F \in \mathcal{F}_h^0.$$

We extend the definition of the jumps to $F \in \mathcal{F}_h^\partial$, by $[\![\boldsymbol{w}]\!] := \boldsymbol{n} \times (\boldsymbol{w} - \boldsymbol{w}^{ext})$, where $\boldsymbol{w}^{ext}$ is the exterior trace.

The finite dimensional spaces we are going to use are of the form

$$\begin{aligned}
\boldsymbol{V}_h &:= \{\boldsymbol{v} \in \boldsymbol{L}^2(\Omega) : \ \ \boldsymbol{v}|_K \in \boldsymbol{V}(K) \ \ \forall K \in \mathcal{T}_h\},\\
\boldsymbol{W}_h &:= \{\boldsymbol{w} \in \boldsymbol{L}^2(\Omega) : \ \boldsymbol{v}|_K \in \boldsymbol{W}(K) \ \forall K \in \mathcal{T}_h\},\\
\boldsymbol{M}_h &:= \{\boldsymbol{\eta} \in \boldsymbol{L}^2(\mathcal{F}_h) : \boldsymbol{\eta}|_F \in \boldsymbol{M}(F) \ \ \forall F \in \mathcal{F}_h\}.
\end{aligned}$$

As indicated in Section 2.1, we incorporate the boundary condition into the spaces by setting

$$\begin{aligned}
\boldsymbol{V}_h^{ext}(\boldsymbol{g}) &:= \{\boldsymbol{v} \in \boldsymbol{V}_h : \ \ \boldsymbol{n} \times \boldsymbol{v}^{ext} = \boldsymbol{g} \text{ on } \Gamma\},\\
\boldsymbol{W}_h^{ext}(\boldsymbol{g}) &:= \{\boldsymbol{w} \in \boldsymbol{W}_h : \boldsymbol{n} \times \boldsymbol{w}^{ext} = \boldsymbol{g} \text{ on } \Gamma\},\\
\boldsymbol{M}_h(\boldsymbol{g}) &:= \{\boldsymbol{\eta} \in \boldsymbol{M}_h : \ \boldsymbol{n} \times \boldsymbol{\eta} = \boldsymbol{g} \text{ on } \Gamma\}.
\end{aligned}$$

These spaces are used to define the DG and HDG methods. To define mixed methods, we use spaces of the form

$$\boldsymbol{V}_h^{\mathrm{curl}} := \boldsymbol{V}_h \cap \mathsf{H}(\mathrm{curl};\Omega) \quad \text{ and } \quad \mathrm{W}_{\mathrm{h}}^{\mathrm{curl}} := \boldsymbol{W}_h \cap \mathsf{H}(\mathrm{curl};\Omega).$$

The spaces with the superscript "curl" are usually called the spaces of edge elements, see [48] and [46]. Examples of the local spaces $\boldsymbol{V}(K)$, $\boldsymbol{W}(K)$ and $\boldsymbol{M}(F)$ can be found in Section 3.4; see also Table 5.

3.2. The weak formulations

For mixed methods of the $\boldsymbol{E}$-$\boldsymbol{H}$ formulation, the approximation $(\boldsymbol{E}_h, \boldsymbol{H}_h)$ is taken in $\boldsymbol{V}_h^{ext}(\boldsymbol{g}_{\boldsymbol{E}}) \times \boldsymbol{W}_h^{\mathrm{curl}}$ and is required to satisfy the equations

$$\begin{aligned}
(\epsilon\, \dot{\boldsymbol{E}}_h, \boldsymbol{v})_{\mathcal{T}_h} - (\nabla \times \boldsymbol{H}_h, \boldsymbol{v})_{\mathcal{T}_h} &= -(\boldsymbol{J}, \boldsymbol{v})_{\mathcal{T}_h} \quad \forall \boldsymbol{v} \in \boldsymbol{V}_h, && \text{(5a)}\\
(\mu\, \dot{\boldsymbol{H}}_h, \boldsymbol{r})_{\mathcal{T}_h} + (\boldsymbol{E}_h, \nabla \times \boldsymbol{r})_{\mathcal{T}_h} + \langle \boldsymbol{n} \times \boldsymbol{E}_h^{ext}, \boldsymbol{r}\rangle_\Gamma &= 0 \qquad\qquad\qquad \forall \boldsymbol{r} \in \boldsymbol{W}_h^{\mathrm{curl}}. && \text{(5b)}
\end{aligned}$$

For the DG and HDG methods, we take the approximation $(\boldsymbol{E}_h, \boldsymbol{H}_h)$ in $\boldsymbol{V}_h \times \boldsymbol{W}_h$ and define them as the solution of

$$\begin{aligned}
(\epsilon\, \dot{\boldsymbol{E}}_h, \boldsymbol{v})_{\mathcal{T}_h} - (\boldsymbol{H}_h, \nabla \times \boldsymbol{v})_{\mathcal{T}_h} - \langle \boldsymbol{n} \times \widehat{\boldsymbol{H}}_h, \boldsymbol{v}\rangle_{\partial\mathcal{T}_h} &= -(\boldsymbol{J}, \boldsymbol{v})_{\mathcal{T}_h} \quad \forall \boldsymbol{v} \in \boldsymbol{V}_h, && \text{(6a)}\\
(\mu\, \dot{\boldsymbol{H}}_h, \boldsymbol{r})_{\mathcal{T}_h} + (\boldsymbol{E}_h, \nabla \times \boldsymbol{r})_{\mathcal{T}_h} + \langle \boldsymbol{n} \times \widehat{\boldsymbol{E}}_h, \boldsymbol{r}\rangle_{\partial\mathcal{T}_h} &= 0 \qquad\qquad\qquad \forall \boldsymbol{r} \in \boldsymbol{W}_h, && \text{(6b)}
\end{aligned}$$

where the tangential components of the numerical traces $(\widehat{\boldsymbol{E}}_h, \widehat{\boldsymbol{H}}_h)$ approximate the tangential components of $(\boldsymbol{E}|_{\mathcal{F}_h}, \boldsymbol{H}|_{\mathcal{F}_h})$ and must be suitably defined, see Table 4. Note that on the boundary of Ω, $\boldsymbol{n} \times \widehat{\boldsymbol{E}}_h = \boldsymbol{n} \times \boldsymbol{E}^{ext}$. Furthermore, the numerical trace $\widehat{\boldsymbol{E}}_h$ has to satisfy the additional equation (9) to ensure the single-valuedness of the numerical trace $\widehat{\boldsymbol{H}}_h$.

For mixed methods of the $\boldsymbol{E}$-$\boldsymbol{A}$ formulation, the approximation $(\boldsymbol{E}_h, \boldsymbol{A}_h, \boldsymbol{H}_h)$ is taken in $\boldsymbol{V}_h \times \boldsymbol{V}_h^{ext}(\boldsymbol{g_A}) \times \boldsymbol{W}_h^{\mathrm{curl}}$ and is required to satisfy the equations

$$
\begin{aligned}
(\dot{\boldsymbol{A}}_h, \boldsymbol{v})_{\mathcal{T}_h} + (\boldsymbol{E}_h, \boldsymbol{v})_{\mathcal{T}_h} &= 0 && \forall \boldsymbol{v} \in \boldsymbol{V}_h, && \text{(7a)}\\
(\epsilon\, \dot{\boldsymbol{E}}_h, \boldsymbol{v})_{\mathcal{T}_h} - (\nabla \times \boldsymbol{H}_h, \boldsymbol{v})_{\mathcal{T}_h} &= -(\boldsymbol{J}, \boldsymbol{v})_{\mathcal{T}_h} && \forall \boldsymbol{v} \in \boldsymbol{V}_h, && \text{(7b)}\\
(\mu \boldsymbol{H}_h, \boldsymbol{r})_{\mathcal{T}_h} - (\boldsymbol{A}_h, \nabla \times \boldsymbol{r})_{\mathcal{T}_h} - \langle \boldsymbol{n} \times \boldsymbol{A}_h^{ext}, \boldsymbol{r}\rangle_\Gamma &= 0 && \forall \boldsymbol{r} \in \boldsymbol{W}_h^{\mathrm{curl}}, && \text{(7c)}
\end{aligned}
$$

For the HDG and DG methods, we take $(\boldsymbol{E}_h, \boldsymbol{A}_h, \boldsymbol{H}_h)$ in the approximation spaces $\boldsymbol{V}_h \times \boldsymbol{V}_h \times \boldsymbol{W}_h$ and define it as the solutions of

$$
\begin{aligned}
(\dot{\boldsymbol{A}}_h, \boldsymbol{v})_{\mathcal{T}_h} + (\boldsymbol{E}_h, \boldsymbol{v})_{\mathcal{T}_h} &= 0 && \forall \boldsymbol{v} \in \boldsymbol{V}_h, && \text{(8a)}\\
(\epsilon\, \dot{\boldsymbol{E}}_h, \boldsymbol{v})_{\mathcal{T}_h} - (\boldsymbol{H}_h, \nabla \times \boldsymbol{v})_{\mathcal{T}_h} - \langle \boldsymbol{n} \times \widehat{\boldsymbol{H}}_h, \boldsymbol{v}\rangle_{\partial\mathcal{T}_h} &= -(\boldsymbol{J}, \boldsymbol{v})_{\mathcal{T}_h} && \forall \boldsymbol{v} \in \boldsymbol{V}_h, && \text{(8b)}\\
(\mu \boldsymbol{H}_h, \boldsymbol{r})_{\mathcal{T}_h} - (\boldsymbol{A}_h, \nabla \times \boldsymbol{r})_{\mathcal{T}_h} - \langle \boldsymbol{n} \times \widehat{\boldsymbol{A}}_h, \boldsymbol{r}\rangle_{\partial\mathcal{T}_h} &= 0 && \forall \boldsymbol{r} \in \boldsymbol{W}_h, && \text{(8c)}
\end{aligned}
$$

where the tangential components of the numerical traces $(\widehat{\boldsymbol{A}}_h, \widehat{\boldsymbol{H}}_h)$ approximate the tangential components of $(\boldsymbol{A}|_{\mathcal{F}_h}, \boldsymbol{H}|_{\mathcal{F}_h})$ and must be suitably defined, see Table 4. [Furthermore, $\widehat{\boldsymbol{A}}_h$ satisfies an additional equation which is similar to (9) with $\widehat{\boldsymbol{A}}_h$ as the element of $\boldsymbol{M}_h(\boldsymbol{g_A})$.](to-be-deleted)

3.3. The numerical traces

The numerical traces for the HDG and DG methods are list in Table 4. Note that they incorporate the boundary conditions and that some of numerical traces are defined in terms of $\boldsymbol{P_M}$, the L^2 projection into $\prod_{K\in\mathcal{T}_h}\prod_{F\in\partial K}\boldsymbol{M}(F)$. Note also that only the tangential component of the numerical traces is seen by the schemes.

Table 4: Exterior and numerical traces: Mixed (top row), HDG (middle row) and DG (bottom row) methods.

	$\boldsymbol{E}$-$\boldsymbol{H}$ formulation	$\boldsymbol{E}$-$\boldsymbol{A}$ formulation
on $\mathcal{F}_h^\partial$:	$\boldsymbol{n} \times \boldsymbol{E}_h^{ext} = \boldsymbol{g_E}$	$\boldsymbol{n} \times \boldsymbol{A}_h^{ext} = \boldsymbol{g_A}$
on $\partial\mathcal{T}_h$:	$\widehat{\boldsymbol{E}}_h \in \boldsymbol{M}_h(\boldsymbol{g_E})$ is a new unknown: $\boldsymbol{n} \times (\widehat{\boldsymbol{H}}_h - \boldsymbol{H}_h) = -\tau(\boldsymbol{P_M}\boldsymbol{E}_h - \widehat{\boldsymbol{E}}_h)$	$\widehat{\boldsymbol{A}}_h \in \boldsymbol{M}_h(\boldsymbol{g_A})$ is a new unknown: $\boldsymbol{n} \times (\widehat{\boldsymbol{H}}_h - \boldsymbol{H}_h) = \tau(\boldsymbol{P_M}\boldsymbol{A}_h - \widehat{\boldsymbol{A}}_h)$
on $\mathcal{F}_h^0$:	$\widehat{\boldsymbol{H}}_h = \{\!\{\boldsymbol{H}_h\}\!\} + C_{11}[\![\boldsymbol{E}_h]\!] + \underline{\boldsymbol{C}}_{12}^T[\![\boldsymbol{H}_h]\!]$ $\widehat{\boldsymbol{E}}_h = \{\!\{\boldsymbol{E}_h\}\!\} + \underline{\boldsymbol{C}}_{12}[\![\boldsymbol{E}_h]\!] - C_{22}\,[\![\boldsymbol{H}_h]\!]$	$\widehat{\boldsymbol{H}}_h = \{\!\{\boldsymbol{H}_h\}\!\} - C_{11}[\![\boldsymbol{A}_h]\!] + \underline{\boldsymbol{C}}_{12}^T[\![\boldsymbol{H}_h]\!]$ $\widehat{\boldsymbol{A}}_h = \{\!\{\boldsymbol{A}_h\}\!\} + \underline{\boldsymbol{C}}_{12}[\![\boldsymbol{A}_h]\!] + C_{22}\,[\![\boldsymbol{H}_h]\!]$
on $\mathcal{F}_h^\partial$:	$\widehat{\boldsymbol{H}}_h = \boldsymbol{H}_h + C_{11}\ \boldsymbol{n}\times(\boldsymbol{E}_h - \widehat{\boldsymbol{E}}_h)$ $\boldsymbol{n} \times \widehat{\boldsymbol{E}}_h = \boldsymbol{g_E}$	$\widehat{\boldsymbol{H}}_h = \boldsymbol{H}_h - C_{11}\ \boldsymbol{n}\times(\boldsymbol{A}_h - \widehat{\boldsymbol{A}}_h)$ $\boldsymbol{n} \times \widehat{\boldsymbol{A}}_h = \boldsymbol{g_A}$

Finally, as it is typical for the HDG methods, the new unknown can be obtained either explicitly as a function of $(\boldsymbol{E}_h, \boldsymbol{H}_h)$ or as the solution of a global system obtained by imposing the single-valuedness of the tangential component

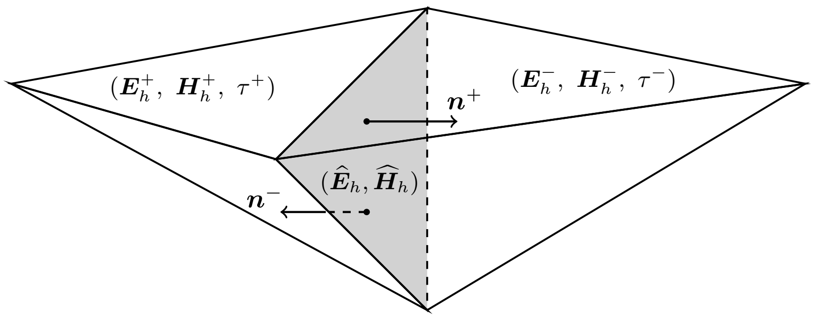

Figure 1: Solution, traces, and stabilization function around an interior face $F \in \mathcal{F}_h^0$.

of the other numerical trace [15]. Specifically we define the numerical trace $\widehat{\boldsymbol{E}}_h$ as the element of $\boldsymbol{M}_h(\boldsymbol{g_E})$ for which the tangential component of the numerical trace $\widehat{\boldsymbol{H}}_h$ is single-valued, that is,

$$\langle \boldsymbol{n} \times \widehat{\boldsymbol{H}}_h, \boldsymbol{\eta} \rangle_{\partial\mathcal{T}_h \setminus \Gamma} \;=\; 0 \qquad \forall \boldsymbol{\eta} \in \boldsymbol{M}_h. \tag{9}$$

If τ is a simple multiplication by a constant on each face, the explicit solution of the above equation can be easily found, see Appendix A, to be the following:

$$\begin{aligned}
\widehat{\boldsymbol{E}}_h &= \frac{Y^+(\boldsymbol{P}_M\boldsymbol{E}_h)^+ + Y^-(\boldsymbol{P}_M\boldsymbol{E}_h)^-}{Y^+ + Y^-} - \frac{[\![\boldsymbol{H}_h]\!]}{Y^+ + Y^-} \qquad \text{where } Y := \tau,\\
\widehat{\boldsymbol{H}}_h &= \frac{Z^+(\boldsymbol{H}_h)^+ + Z^-(\boldsymbol{H}_h)^-}{Z^+ + Z^-} + \frac{[\![\boldsymbol{P}_M\boldsymbol{E}_h]\!]}{Z^+ + Z^-} \qquad \text{where } Z := \tau^{-1}.
\end{aligned}$$

To enforce the stability of the space-discretization, it is enough to require that τ be positive. If ϵ and μ are piecewise constant, and we set $\tau := \sqrt{\epsilon/\mu}$, Z becomes the impedance, Y the admittance, and the numerical traces $\widehat{\boldsymbol{E}}_h$ and $\widehat{\boldsymbol{H}}_h$ become (a generalization of the case in which $\boldsymbol{P_M}$ is the identity of) the well known upwinding numerical traces.

For the classic DG methods, we consider the particular case in which C_{11}, C_{22} are scalars and $\underline{\boldsymbol{C}}_{12}$ is a matrix. Stability is achieved when C_{11} and C_{22} are non-negative. There are three popular cases covered by this anzatz. The first is the *upwinding* numerical traces, as they are obtained by taking

$$C_{11} = 1/(Z^+ + Z^-),\ C_{22} = 1/(Y^+ + Y^-),$$

and defining the matrix $\underline{\boldsymbol{C}}_{12}$ by $\underline{\boldsymbol{C}}_{12}\boldsymbol{v} = -\frac{Y^+\boldsymbol{n}^+ + Y^-\boldsymbol{n}^-}{2(Y^+ + Y^-)} \times \boldsymbol{v} = +\frac{Z^+\boldsymbol{n}^+ + Z^-\boldsymbol{n}^-}{2(Z^+ + Z^-)} \times \boldsymbol{v}$; note that $\underline{\boldsymbol{C}}_{12}$ is skew-symmetric in this case. Another choice is obtained by setting $C_{11} = C_{22} = 0$ and taking the matrix $\underline{\boldsymbol{C}}_{12}$ such that, on the interior faces, we get

$$\widehat{\boldsymbol{E}}_h = \theta(\boldsymbol{E}_h^t)^+ + (1-\theta)(\boldsymbol{E}_h^t)^-, \quad \widehat{\boldsymbol{H}}_h = \theta(\boldsymbol{H}_h^t)^- + (1-\theta)(\boldsymbol{H}_h^t)^+,$$

for some $\theta \in [0,1]$ depending on the face. These are the so-called *alternating* traces. A third choice is $C_{11} = C_{22} = 0$ and $\underline{\boldsymbol{C}}_{12} = 0$ which gives rise to the so-called centered traces.

3.4. Examples of finite element spaces

Here we discuss some specific choices for the local spaces $\boldsymbol{V}(K)$, $\boldsymbol{W}(K)$, and $\boldsymbol{M}(F)$, which are then used to construct the global approximation spaces $\boldsymbol{V}_h$, $\boldsymbol{W}_h$, and $\boldsymbol{M}_h$. These choices are summarized in Table 5. Therein, $\boldsymbol{\mathcal{P}}_\ell = \boldsymbol{\mathcal{P}}_\ell(K)$ denotes the space of vector-valued functions whose components are polynomials of degree ℓ on the element K. The space $\boldsymbol{\mathcal{P}}_\ell^t = \boldsymbol{\mathcal{P}}_\ell^t(F)$ denotes the space of vector-valued functions which are tangent to the face F and whose components are polynomials of degree ℓ on the element F. The space $\widetilde{\boldsymbol{\mathcal{P}}}_\ell$ is the space of homogeneous polynomials of degree ℓ on each component. The space $\widetilde{\mathcal{P}}_\ell$ is the space of homogeneous polynomials of degree ℓ. Finally, the symbol ∇_F denotes the tangential gradient on the face F.

Table 5: Examples of finite dimensional spaces.

	K	$\boldsymbol{V}(K)$	$\boldsymbol{W}(K)$	$\boldsymbol{M}(F)$	k	global spaces
			mixed methods			
[43]	tetrahedron	$\boldsymbol{\mathcal{P}}_k$	$\boldsymbol{\mathcal{P}}_k \oplus (\boldsymbol{x} \times \widetilde{\boldsymbol{\mathcal{P}}}_k)$	–	$\geqslant 0$	$\boldsymbol{V}_h \times \boldsymbol{W}_h^{\text{curl}}$
	tetrahedron	$\boldsymbol{\mathcal{P}}_k$	$\boldsymbol{\mathcal{P}}_{k+1}$	–	$\geqslant 1$	$\boldsymbol{V}_h \times \boldsymbol{W}_h^{\text{curl}}$
			HDG methods			
[15]	polyhedron	$\boldsymbol{\mathcal{P}}_k$	$\boldsymbol{\mathcal{P}}_k$	$\boldsymbol{\mathcal{P}}_k^t$	$\geqslant 0$	$\boldsymbol{V}_h \times \boldsymbol{W}_h$
[12]	polyhedron	$\boldsymbol{\mathcal{P}}_{k+1}$	$\boldsymbol{\mathcal{P}}_k$	$\boldsymbol{\mathcal{P}}_k^t \oplus \nabla_F \widetilde{\mathcal{P}}_{k+2}$	$\geqslant 1$	$\boldsymbol{V}_h \times \boldsymbol{W}_h$
[23]	polyhedron	$\boldsymbol{\mathcal{P}}_{k+1}$	$\boldsymbol{\mathcal{P}}_k$	$\boldsymbol{\mathcal{P}}_{k+1}^t$	$\geqslant 0$	$\boldsymbol{V}_h \times \boldsymbol{W}_h$
			DG methods			
[30, 13]	polyhedron	$\boldsymbol{\mathcal{P}}_k$	$\boldsymbol{\mathcal{P}}_k$	-	$\geqslant 0$	$\boldsymbol{V}_h \times \boldsymbol{W}_h$

For mixed methods, the space of traces $\boldsymbol{M}$ is not needed since $\boldsymbol{H}(\text{curl})$-conformity is enforced by the construction of the approximation space $\boldsymbol{W}_h^{\text{curl}}$. Mixed methods are not limited to simplicial meshes since general $\boldsymbol{H}(\text{curl})$-conforming elements can be constructed for hexahedra, prisms, and pyramids, see [16], by using exact sequences.

For HDG methods, relatively fewer references exist for the time-dependent Maxwell's equations, compared to the time-harmonic or the static case. For the time-dependent case, a typical choice is to use $\mathcal{P}_k$ for all approximations including the numerical trace; see, for instance, [15]. For the steady-state case, various choices of the approximation spaces exist and we refer to [23] for an introduction where a unified analysis is established to investigate the different convergence properties of the various choices. For DG methods, the trace space $\boldsymbol{M}$ becomes unnecessary since no hybrid unknown needs to be introduced. To the best of our knowledge, all DG methods use the space of polynomials $\boldsymbol{\mathcal{P}}_k$ for both the approximations of $\boldsymbol{E}_h$ and $\boldsymbol{H}_h$; see, for instance, [30, 13].

3.5. The initial conditions

We describe how to compute the initial conditions from the initial data

$\boldsymbol{E}_0, \boldsymbol{H}_0$. For the methods associated with the $\boldsymbol{E}$-$\boldsymbol{H}$ formulation, we can simply take the initial conditions as the $\boldsymbol{L}^2$-projections of $\boldsymbol{E}_0$ and $\boldsymbol{H}_0$ into the corresponding spaces.

For the methods associated with the $\boldsymbol{E}$-$\boldsymbol{A}$ formulation, the initial condition for the electric field can be taken as the $\boldsymbol{L}^2$-projection of $\boldsymbol{E}_0$ into the corresponding space. In contrast, the definition of the initial condition for the magnetic potential is more involved since the initial data for $\boldsymbol{A}$ is not given and $\epsilon\boldsymbol{A}$ is divergence-free. We define the initial condition for $(\boldsymbol{H}, \boldsymbol{A})$ as an approximation to the solution of the system

$$
\begin{aligned}
\mu\boldsymbol{H} - \nabla \times \boldsymbol{A} &= 0 && \text{in } \Omega, && \text{(10a)}\\
\nabla \times \boldsymbol{H} + \epsilon\nabla p &= \nabla \times \boldsymbol{H}_0 && \text{in } \Omega, && \text{(10b)}\\
\nabla \cdot \epsilon\boldsymbol{A} &= 0 && \text{in } \Omega, && \text{(10c)}\\
\boldsymbol{n} \times \boldsymbol{A} &= \boldsymbol{g}_{\boldsymbol{A}} && \text{on } \Gamma, && \text{(10d)}\\
p &= 0 && \text{on } \Gamma, && \text{(10e)}
\end{aligned}
$$

where p is a Lagrange multiplier introduced to enforce the divergence-free condition on $\epsilon\boldsymbol{A}$ explicitly. This auxiliary pressure turns out to be zero since $\nabla \times \boldsymbol{H}_0$ is divergence-free.

The approximation $(\boldsymbol{H}_h, \boldsymbol{A}_h, p_h, \widehat{\boldsymbol{A}}_h, \widehat{p}_h)$ is taken in the space $\boldsymbol{W}_h \times \boldsymbol{V}_h \times Q_h \times \boldsymbol{M}_h(\boldsymbol{g}_{\boldsymbol{A}}) \times M_h^n$ as the solution of the following system

$$
\begin{aligned}
(\mu\boldsymbol{H}_h, \boldsymbol{r})_{\mathcal{T}_h} - (\boldsymbol{A}_h, \nabla \times \boldsymbol{r})_{\mathcal{T}_h} - \langle \widehat{\boldsymbol{A}}_h, \boldsymbol{r} \times \boldsymbol{n}\rangle_{\partial\mathcal{T}_h} &= 0 && \text{(11a)}\\
(\boldsymbol{H}_h, \nabla \times \boldsymbol{v})_{\mathcal{T}_h} + \langle \boldsymbol{n} \times \widehat{\boldsymbol{H}}_h, \boldsymbol{v}\rangle_{\partial\mathcal{T}_h} - (\epsilon\, p_h, \nabla \cdot \boldsymbol{v})_{\mathcal{T}_h} + \langle \epsilon\, \widehat{p}_h, \boldsymbol{v} \cdot \boldsymbol{n}\rangle_{\partial\mathcal{T}_h} & && \text{(11b)}\\
&= (\nabla \times \boldsymbol{H}_0, \boldsymbol{v})_{\mathcal{T}_h}\\
-(\epsilon\boldsymbol{A}_h, \nabla q)_{\mathcal{T}_h} + \langle \boldsymbol{A}_h \cdot \boldsymbol{n} + \tau_n(p_h - \widehat{p}_h), \epsilon\, q\rangle_{\partial\mathcal{T}_h} &= 0 && \text{(11c)}\\
\langle \boldsymbol{A}_h \cdot \boldsymbol{n} + \tau_n(p_h - \widehat{p}_h), \lambda\rangle_{\partial\mathcal{T}_h\setminus\Gamma} &= 0 && \text{(11d)}\\
\langle \boldsymbol{n} \times \widehat{\boldsymbol{H}}_h, \boldsymbol{\eta}\rangle_{\partial\mathcal{T}_h\setminus\Gamma} &= 0 && \text{(11e)}\\
\langle \widehat{p}_h, \lambda\rangle_{\Gamma} &= 0 && \text{(11f)}
\end{aligned}
$$

for all $(\boldsymbol{r}, \boldsymbol{v}, q, \boldsymbol{\eta}, \lambda) \in \boldsymbol{W}_h \times \boldsymbol{V}_h \times Q_h \times \boldsymbol{M}_h \times M_h^n$, where τ_n is a stabilization parameter and the scalar spaces have the form

$$
\begin{aligned}
Q_h &:= \{q \in L^2(\Omega) : \, q|_K \in Q(K), \, \forall K \in \mathcal{T}_h\},\\
M_h^n &:= \{\lambda \in L^2(\mathcal{F}_h) : \, \lambda|_F \in M^n(F), \, \forall F \in \mathcal{F}_h\},
\end{aligned}
$$

where $Q(K)$ and $M^n(F)$ are local scalar-valued polynomial spaces. The definition of the initial solution for the mixed and the DG methods is similar.

Remark 3.1. *In our numerical experiments, we use the following choices of the local spaces for the variant* k

$$
\boldsymbol{V}(K) \times \boldsymbol{W}_k \times \boldsymbol{M}(F) \times Q(K) \times M^n(F) = \boldsymbol{\mathcal{P}}_k \times \boldsymbol{\mathcal{P}}_k \times \boldsymbol{\mathcal{P}}_k^t \times \mathcal{P}_k \times \mathcal{P}_k
$$

and for the variant $\mathfrak{B}$

$$\boldsymbol{V}(K) \times \boldsymbol{W}_k \times \boldsymbol{M}(F) \times Q(K) \times M^n(F) = \boldsymbol{\mathcal{P}}_{k+1} \times \boldsymbol{\mathcal{P}}_k \times \boldsymbol{\mathcal{P}}^t_{k+1} \times \mathcal{P}_k \times \mathcal{P}_{k+1}$$

What we call the "variant k" is the standard HDG method with all variables using piecewise polynomials of degree k, [15]. What we call "Variant $\mathfrak{B}$*" is the HDG method introduced in [23] where the authors study four optimal variants of the HDG method for the frequency domain Maxwell equations.*

4. Hamiltonian structure of the semidiscrete methods

In this section, we prove the Hamiltonian structure of the semidiscrete schemes based on the $\boldsymbol{E}$-$\boldsymbol{H}$ and the $\boldsymbol{E}$-$\boldsymbol{A}$ formulations. From now on, we use the subscript $\bigstar$ on the Poisson brackets to differentiate between the $\boldsymbol{E}$-$\boldsymbol{H}$ formulation, $\bigstar = \mathcal{E}$, and the $\boldsymbol{E}$-$\boldsymbol{A}$ formulation, $\bigstar = w$. When we simply write $\bigstar$, it means that both formulations can be used. Similarly, we use the superscript $*$ to differentiate between the methods. So, for the mixed method, we use $* = M$, for the DG method, $* = DG$, and for the HDG method, $* = HDG$. When we simply write $*$, we refer to any of the above methods.

We claim that the semidiscrete methods presented in Section 3 define a Hamiltonian dynamical system for which

(i) the discrete phase and test space $(\mathcal{M}_h, \mathcal{D}_h)$ is an approximation to its continuous counterpart $(\mathcal{M}, \mathcal{D})$,

(ii) the Poisson bracket $\{\cdot,\cdot\}_{\bigstar,h}$ is a discrete version of $\{\cdot,\cdot\}_{\bigstar}$,

(iii) the Hamiltonian $\mathcal{H}^*_{\bigstar,h}$ is a discrete version of the Hamiltonian $\mathcal{H}^*_{\star}$.

We divide this section into two parts. In the first part, we investigate the $\boldsymbol{E}$-$\boldsymbol{H}$ formulation of the mixed, DG and HDG methods. We shall show that the mixed methods have a natural Hamiltonian structure and that the DG methods become Hamiltonian when the coefficients C_{11} and C_{22} defining their numerical traces, see Table 4, are equal to zero. Consequently, the mixed and DG methods conserve their corresponding discrete energy $\mathcal{H}^M_{\mathcal{E},h}$ and $\mathcal{H}^{DG}_{\mathcal{E},h}$, respectively. As a consequence, the discrete electric and the magnetic charges are also conserved. On the other hand, the restriction on the DG methods to be Hamiltonian, namely, that $C_{11} = C_{22} = 0$, immediately implies, see Appendix B, that the HDG methods do <u>not</u> possess a Hamiltonian structure. This is consistent with the fact that their discrete energy always decreases in time.

In the second part, we consider the $\boldsymbol{E}$-$\boldsymbol{A}$ formulation of the mixed, DG and HDG methods. We shall prove that all three methods have a Hamiltonian structure. Consequently, their discrete Hamiltonian energy $\mathcal{H}^M_{w,h}$, $\mathcal{H}^{DG}_{w,h}$, and $\mathcal{H}^{HDG}_{w,h}$ are conserved in time evolution. In addition, we prove that, as it holds in the continuous case, the electric and the magnetic charges are also conserved in the discrete level. This is achieved by exploiting the discrete Hamiltonian structure of these numerical methods.

4.1. The electric and magnetic field formulation

We begin by describing each of the components of the Hamiltonian structure for the methods defined by using the $\boldsymbol{E}$-$\boldsymbol{H}$ formulation:

(i) phase and test function spaces

$$\begin{array}{llll}
\text{mixed:} & \mathcal{M}_h^M := \boldsymbol{V}_h^{ext}(\boldsymbol{g_E})\times\boldsymbol{W}_h^{\mathrm{curl}} & \text{and} & \mathcal{D}_h^M := \boldsymbol{V}_h^{ext}(\boldsymbol{0})\times\boldsymbol{W}_h^{\mathrm{curl}}, \\
\text{DG:} & \mathcal{M}_h^{DG} := \boldsymbol{V}_h^{ext}(\boldsymbol{g_E})\times\boldsymbol{W}_h & \text{and} & \mathcal{D}_h^{DG} := \boldsymbol{V}_h^{ext}(\boldsymbol{0})\times\boldsymbol{W}_h, \\
\text{HDG:} & \mathcal{M}_h^{HDG} := \boldsymbol{V}_h^{ext}(\boldsymbol{g_E})\times\boldsymbol{W}_h & \text{and} & \mathcal{D}_h^{HDG} := \boldsymbol{V}_h^{ext}(\boldsymbol{0})\times\boldsymbol{W}_h.
\end{array}$$

(ii) Poisson bracket

$$\begin{aligned}
\{F,G\}_{\mathcal{E},h} = \; & \Big(\frac{1}{\epsilon}\frac{\delta F}{\delta \boldsymbol{E}_h}, \nabla\times\Big(\frac{1}{\mu}\frac{\delta G}{\delta \boldsymbol{H}_h}\Big)\Big)_{\mathcal{T}_h} - \Big(\frac{1}{\epsilon}\frac{\delta G}{\delta \boldsymbol{E}_h}, \nabla\times\Big(\frac{1}{\mu}\frac{\delta F}{\delta \boldsymbol{H}_h}\Big)\Big)_{\mathcal{T}_h} \\
& - \langle\frac{1}{\epsilon}\breve{\frac{\delta F}{\delta \boldsymbol{E}_h}}, \boldsymbol{n}\times\Big(\frac{1}{\mu}\frac{\delta G}{\delta \boldsymbol{H}_h}\Big)\rangle_{\partial\mathcal{T}_h} + \langle\frac{1}{\epsilon}\breve{\frac{\delta G}{\delta \boldsymbol{E}_h}}, \boldsymbol{n}\times\Big(\frac{1}{\mu}\frac{\delta F}{\delta \boldsymbol{H}_h}\Big)\rangle_{\partial\mathcal{T}_h},
\end{aligned}$$

where

$$\breve{\boldsymbol{u}} := \begin{cases} \{\!\{\boldsymbol{u}\}\!\} + \underline{\boldsymbol{C}}_{12}[\![\boldsymbol{u}]\!] & F\in\mathcal{F}_h^0, \\ \boldsymbol{u}^{ext} & F\in\mathcal{F}_h^\partial, \end{cases}$$

(iii) Hamiltonian

$$\mathcal{H}_{\mathcal{E},h} = \frac{1}{2}\left((\epsilon\,\boldsymbol{E}_h,\,\boldsymbol{E}_h)_{\mathcal{T}_h} + (\mu\,\boldsymbol{H}_h,\,\boldsymbol{H}_h)_{\mathcal{T}_h}\right) - (\boldsymbol{J}_\times, \mu\boldsymbol{H}_h),$$

(iv) and coordinate functionals

$$F_{\boldsymbol{E}_h} = (\epsilon\,\boldsymbol{E}_h, \boldsymbol{v})_{\mathcal{T}_h} \quad\text{and}\quad F_{\boldsymbol{H}_h} = (\mu\,\boldsymbol{H}_h, \boldsymbol{r})_{\mathcal{T}_h} \qquad \forall\,(\boldsymbol{v},\boldsymbol{r})\in\mathcal{D}_h^*.$$

We can now state and prove the main result of this subsection.

Theorem 4.1 (Hamiltonian structure of the $\boldsymbol{E}$-$\boldsymbol{H}$ formulation). *We have that*

(i) *The mixed method* (5) *defines a Hamiltonian dynamical system with*

$$(\mathcal{M}_h^M, \{\cdot,\cdot\}_{\mathcal{E},h}, \mathcal{H}_{\mathcal{E},h}).$$

(ii) *The DG method* (6), *with numerical fluxes defined by Table 4, defines a Hamiltonian dynamical system with*

$$(\mathcal{M}_h^{DG}, \{\cdot,\cdot\}_{\mathcal{E},h}, \mathcal{H}_{\mathcal{E},h}),$$

if and only if $C_{11} = C_{22} = 0$.

(iii) *The HDG method* (6)*, with numerical fluxes defined by Table 4, is such that*

$$(\mathcal{M}_h^{HDG}, \{\cdot,\cdot\}_{\mathcal{E},h}, \mathcal{H}_{\mathcal{E},h}),$$

is never a Hamiltonian dynamical system.

This result is similar to [63] for DG methods. We include the proof in Appendix B for completeness.

A straightforward corollary of this result are the following conservation laws. The proof is included in Appendix C

Corollary 4.1 (discrete conservation). *The mixed method* (5) *and the DG method* (6) *with numerical traces defined by Table 4 satisfy the following conservation laws.*

$$\begin{aligned} \textit{(electric charge)} \qquad (\epsilon\dot{\boldsymbol{E}}_h, \nabla v)_{\mathcal{T}_h} &= 0, \\ \textit{(magnetic charge)} \qquad (\mu\dot{\boldsymbol{H}}_h, \nabla w)_{\mathcal{T}_h} &= 0, \\ \textit{(energy)} \qquad \dot{\mathcal{H}}_{\mathcal{E},h} &= 0, \end{aligned}$$

for all test functions $v, w \in H_0^1(\Omega)$ satisfying $(\nabla v, \nabla w) \in \mathcal{D}_h^*$ where $* = M$ for the mixed method, and $* = DG$ for the DG method.

4.2. The electric and magnetic vector potential formulation

Let us describe now the components of the Hamiltonian structure for the methods defined by using the $\boldsymbol{E}$-$\boldsymbol{A}$ formulation. In what follows, the superscript $*$ stands for M, DG and HDG. We have:

(i) phase and test function spaces:

$$\mathcal{M}_h^* := \boldsymbol{V}_h \times \boldsymbol{V}_h^{ext}(\boldsymbol{g_A}) \quad \text{and} \quad \mathcal{D}_h^* := \boldsymbol{V}_h \times \boldsymbol{V}_h^{ext}(\boldsymbol{0}). \tag{12a}$$

(ii) Poisson bracket

$$\{F, G\}_{w,h} = \Big(\frac{1}{\epsilon}\frac{\delta F}{\delta \boldsymbol{E}_h}, \frac{\delta G}{\delta \boldsymbol{A}_h}\Big)_{\mathcal{T}_h} - \Big(\frac{1}{\epsilon}\frac{\delta G}{\delta \boldsymbol{E}_h}, \frac{\delta F}{\delta \boldsymbol{A}_h}\Big)_{\mathcal{T}_h}, \tag{12b}$$

(iii) Hamiltonian

$$\begin{aligned} \mathcal{H}_{w,h}^* =& \frac{1}{2}\Big((\epsilon\boldsymbol{E}_h, \boldsymbol{E}_h)_{\mathcal{T}_h} + (\mu\boldsymbol{H}_h, \boldsymbol{H}_h)_{\mathcal{T}_h} + \langle \boldsymbol{n} \times (\widehat{\boldsymbol{H}}_h^* - \boldsymbol{H}_h), \boldsymbol{A}_h - \widehat{\boldsymbol{A}}_h^* \rangle_{\partial\mathcal{T}_h}\Big) \\ &- (\boldsymbol{A}_h, \boldsymbol{J})_{\mathcal{T}_h}, \end{aligned} \tag{12c}$$

(iv) and coordinate functionals given by

$$F_{\boldsymbol{E}_h} = (\epsilon\, \boldsymbol{E}_h, \boldsymbol{v})_{\mathcal{T}_h} \quad \text{and} \quad F_{\boldsymbol{A}_h} = (\epsilon\, \boldsymbol{A}_h, \boldsymbol{v})_{\mathcal{T}_h} \qquad \forall\ (\boldsymbol{v}, \boldsymbol{w}) \in \mathcal{D}_h^*. \tag{12d}$$

The third term of the Hamiltonian, called the stabilization term, reduces to different forms for different discretization methods, as we see in the following result proven in Appendix E.

Proposition 4.1 (The form of the stabilization term). *Set*

$$S_h^*(\boldsymbol{A}_h, \boldsymbol{H}_h) := \langle \boldsymbol{n} \times (\widehat{\boldsymbol{H}}_h^* - \boldsymbol{H}_h), \boldsymbol{A}_h - \widehat{\boldsymbol{A}}_h^* \rangle_{\partial\mathcal{T}_h}.$$

Then

$$\begin{aligned} S_h^M(\boldsymbol{A}_h, \boldsymbol{H}_h) \quad &= 0 \\ S_h^{DG}(\boldsymbol{A}_h, \boldsymbol{H}_h) \quad &= \langle C_{11} [\![\boldsymbol{A}_h]\!], [\![\boldsymbol{A}_h]\!] \rangle_{\mathcal{F}_h} + \langle C_{22} [\![\boldsymbol{H}_h]\!], [\![\boldsymbol{H}_h]\!] \rangle_{\mathcal{F}_h^0}, \\ S_h^{HDG}(\boldsymbol{A}_h, \boldsymbol{H}_h) &= \langle \tau(\boldsymbol{P_M} \boldsymbol{A}_h - \widehat{\boldsymbol{A}}_h) \times \boldsymbol{n}, (\boldsymbol{P_M} \boldsymbol{A}_h - \widehat{\boldsymbol{A}}_h) \times \boldsymbol{n} \rangle_{\partial\mathcal{T}_h}, \end{aligned}$$

We are ready to state and prove our main result.

Theorem 4.2 (Hamiltonian structure of the $\boldsymbol{E}$-$\boldsymbol{A}$ formulation). *We have that*

(i) *The mixed method* (7) *defines a Hamiltonian dynamical system with*

$$(\mathcal{M}_h^M, \{\cdot,\cdot\}_{\omega,h}, \mathcal{H}_{\omega,h}^M).$$

(ii) *The DG method* (8)*, with numerical fluxes defined by Table 4, defines a Hamiltonian dynamical system with*

$$(\mathcal{M}_h^{DG}, \{\cdot,\cdot\}_{\omega,h}, \mathcal{H}_{\omega,h}^{DG}).$$

(iii) *The HDG method* (8)*, with numerical fluxes defined by Table 4, defines a Hamiltonian dynamical system with*

$$(\mathcal{M}_h^{HDG}, \{\cdot,\cdot\}_{\omega,h}, \mathcal{H}_{\omega,h}^{HDG}).$$

To prove this result, we use the following auxiliary result proven in the Appendix F.

Lemma 4.1. *We have*

$$\langle \boldsymbol{n} \times (\delta\widehat{\boldsymbol{H}}_h^* - \delta\boldsymbol{H}_h), \boldsymbol{A}_h - \widehat{\boldsymbol{A}}_h^* \rangle_{\partial\mathcal{T}_h} = \langle \boldsymbol{n} \times (\widehat{\boldsymbol{H}}_h^* - \boldsymbol{H}_h), \delta\boldsymbol{A}_h - \delta\widehat{\boldsymbol{A}}_h^* \rangle_{\partial\mathcal{T}_h}.$$

Proof (Proof of Theorem 4.2). By definition of the coordinate functionals $F_{\boldsymbol{E}_h}$ and $F_{\boldsymbol{A}_h}$, we have that

$$\frac{1}{\epsilon}\frac{\delta F_{\boldsymbol{E}_h}}{\delta \boldsymbol{E}_h} = \boldsymbol{v}, \quad \frac{\delta F_{\boldsymbol{E}_h}}{\delta \boldsymbol{A}_h} = 0, \quad \frac{\delta F_{\boldsymbol{A}_h}}{\delta \boldsymbol{E}_h} = 0, \quad \frac{1}{\epsilon}\frac{\delta F_{\boldsymbol{A}_h}}{\delta \boldsymbol{A}_h} = \boldsymbol{v},$$

and we get, by definition of the Poisson bracket, that

$$\{F_{\boldsymbol{A}_h}, \mathcal{H}_{w,h}^*\}_{\omega,h} = -(\frac{\delta\mathcal{H}_{w,h}^*}{\delta\boldsymbol{E}_h}, \boldsymbol{v})_{\mathcal{T}_h} \quad \text{and} \quad \{F_{\boldsymbol{E}_h}, \mathcal{H}_{w,h}^*\}_{\omega,h} = (\frac{\delta\mathcal{H}_{w,h}^*}{\delta\boldsymbol{A}_h}, \boldsymbol{v})_{\mathcal{T}_h}.$$

So, to show that

$$
\begin{aligned}
(\epsilon\, \dot{\boldsymbol{A}}_h, \boldsymbol{v})_{\mathcal{T}_h} &= \dot{F}_{\boldsymbol{A}_h} = \{F_{\boldsymbol{A}_h},\, \mathcal{H}^*_{w,h}\}_{\omega,h} = -(\epsilon\, \boldsymbol{E}_h, \boldsymbol{v})_{\mathcal{T}_h}, \\
(\epsilon\, \dot{\boldsymbol{E}}_h, \boldsymbol{v})_{\mathcal{T}_h} &= \dot{F}_{\boldsymbol{E}_h} = \{F_{\boldsymbol{E}_h},\, \mathcal{H}^*_{w,h}\}_{\omega,h} = (\boldsymbol{H}_h, \nabla \times \boldsymbol{v})_{\mathcal{T}_h} + \langle \boldsymbol{n} \times \widehat{\boldsymbol{H}}^*_h, \boldsymbol{v}\rangle_{\partial\mathcal{T}_h} - (\boldsymbol{v}, \boldsymbol{J})_{\mathcal{T}_h},
\end{aligned}
$$

we must show that the expressions

$$
\begin{aligned}
\Theta_{\boldsymbol{A}_h} :=& \left(\frac{\delta\mathcal{H}^*_{w,h}}{\delta\boldsymbol{E}_h}, \boldsymbol{v}\right)_{\mathcal{T}_h} - (\epsilon\, \boldsymbol{E}_h, \boldsymbol{v})_{\mathcal{T}_h}, \\
\Theta_{\boldsymbol{E}_h} :=& -\left(\frac{\delta\mathcal{H}^*_{w,h}}{\delta\boldsymbol{A}_h}, \boldsymbol{v}\right)_{\mathcal{T}_h} + (\boldsymbol{H}_h, \nabla \times \boldsymbol{v})_{\mathcal{T}_h} + \langle \boldsymbol{n} \times \widehat{\boldsymbol{H}}^*_h, \boldsymbol{v}\rangle_{\partial\mathcal{T}_h} - (\boldsymbol{v}, \boldsymbol{J})_{\mathcal{T}_h},
\end{aligned}
$$

are both equal to zero.

Now, since $\frac{\delta\mathcal{H}^{DG}_{w,h}}{\delta\boldsymbol{E}_h} = \epsilon\, \boldsymbol{E}_h$, we immediately get that $\Theta_{\boldsymbol{A}_h} = 0$. The proof that $\Theta_{\boldsymbol{E}_h} = 0$ is more difficult because obtaining $\frac{\delta\mathcal{H}^{DG}_{w,h}}{\delta\boldsymbol{A}_h}$ is more involved. We do this next. By the definition of the Hamiltonian $\mathcal{H}^{DG}_{w,h}$, its variation with respect to $\boldsymbol{A}_h$ is

$$
\begin{aligned}
\left(\frac{\delta\mathcal{H}^{DG}_{w,h}}{\delta\boldsymbol{A}_h}, \boldsymbol{\delta A}_h\right)_{\mathcal{T}_h} =& (\mu\, \delta\boldsymbol{H}_h, \boldsymbol{H}_h)_{\mathcal{T}_h} + \frac{1}{2}\delta\langle \boldsymbol{n} \times (\widehat{\boldsymbol{H}}^*_h - \boldsymbol{H}_h), \boldsymbol{A}_h - \widehat{\boldsymbol{A}}^*_h\rangle_{\partial\mathcal{T}_h} - (\delta\boldsymbol{A}_h, \boldsymbol{J})_{\mathcal{T}_h} \\
=& (\mu\, \delta\boldsymbol{H}_h, \boldsymbol{H}_h)_{\mathcal{T}_h} + \langle \boldsymbol{n} \times (\widehat{\boldsymbol{H}}^*_h - \boldsymbol{H}_h), \delta\boldsymbol{A}_h - \delta\widehat{\boldsymbol{A}}^*_h\rangle_{\partial\mathcal{T}_h} - (\delta\boldsymbol{A}_h, \boldsymbol{J})_{\mathcal{T}_h},
\end{aligned}
$$

by Lemma 4.1. Taking the variation on the third equation defining the method, and then setting $\boldsymbol{r} := \boldsymbol{H}_h$, we obtain

$$
\begin{aligned}
(\mu\, \delta\boldsymbol{H}_h, \boldsymbol{H}_h)_{\mathcal{T}_h} =& (\delta\boldsymbol{A}_h, \nabla \times \boldsymbol{H}_h)_{\mathcal{T}_h} + \langle \boldsymbol{n} \times \delta\widehat{\boldsymbol{A}}^*_h, \boldsymbol{H}_h\rangle_{\partial\mathcal{T}_h} \\
=& (\boldsymbol{H}_h, \nabla \times \delta\boldsymbol{A}_h)_{\mathcal{T}_h} + \langle \delta\boldsymbol{A}_h - \delta\widehat{\boldsymbol{A}}^*_h, \boldsymbol{n} \times \boldsymbol{H}_h\rangle_{\partial\mathcal{T}_h} \\
=& (\boldsymbol{H}_h, \nabla \times \delta\boldsymbol{A}_h)_{\mathcal{T}_h} + \langle \boldsymbol{n} \times \widehat{\boldsymbol{H}}^*_h, \delta\boldsymbol{A}_h\rangle_{\partial\mathcal{T}_h} \\
& + \langle \delta\boldsymbol{A}_h - \delta\widehat{\boldsymbol{A}}^*_h, \boldsymbol{n} \times \boldsymbol{H}_h\rangle_{\partial\mathcal{T}_h} - \langle \boldsymbol{n} \times \widehat{\boldsymbol{H}}^*_h, \delta\boldsymbol{A}_h\rangle_{\partial\mathcal{T}_h} \\
=& (\boldsymbol{H}_h, \nabla \times \delta\boldsymbol{A}_h)_{\mathcal{T}_h} + \langle \boldsymbol{n} \times \widehat{\boldsymbol{H}}^*_h, \delta\boldsymbol{A}_h\rangle_{\partial\mathcal{T}_h} \\
& + \langle \delta\boldsymbol{A}_h - \delta\widehat{\boldsymbol{A}}^*_h, \boldsymbol{n} \times (\boldsymbol{H}_h - \widehat{\boldsymbol{H}}^*_h)\rangle_{\partial\mathcal{T}_h},
\end{aligned}
$$

because

$$
\langle \delta\widehat{\boldsymbol{A}}^*_h, \boldsymbol{n} \times \widehat{\boldsymbol{H}}^*_h\rangle_{\partial\mathcal{T}_h} = \langle \delta\widehat{\boldsymbol{A}}^*_h, \boldsymbol{n} \times \widehat{\boldsymbol{H}}^*_h\rangle_{\Gamma} = \langle \delta\boldsymbol{P_M}(\boldsymbol{g_A} \times \boldsymbol{n}), \boldsymbol{n} \times \widehat{\boldsymbol{H}}^*_h\rangle_{\Gamma} = 0.
$$

This implies that

$$
\left(\frac{\delta\mathcal{H}^*_{w,h}}{\delta\boldsymbol{A}_h}, \boldsymbol{\delta A}_h\right)_{\mathcal{T}_h} = (\boldsymbol{H}_h, \nabla \times \delta\boldsymbol{A}_h)_{\mathcal{T}_h} + \langle \boldsymbol{n} \times \widehat{\boldsymbol{H}}^*_h, \delta\boldsymbol{A}_h\rangle_{\partial\mathcal{T}_h} - (\delta\boldsymbol{A}_h, \boldsymbol{J})_{\mathcal{T}_h}, \quad (13)
$$

and so, for any test function $\boldsymbol{v}$ for the magnetic potentials, we can set $\delta\boldsymbol{A}_h := \boldsymbol{v}$ and get that $\Theta_{\boldsymbol{E}_h} = 0$, as desired. This completes the proof.

A straightforward corollary of this result are the following conservation laws.

Corollary 4.2 (discrete conservation). *The mixed method* (7) *and the DG and HDG method* (8) *with numerical traces define by Table 4 satisfy the following conservation laws:*

$$
\begin{aligned}
&\textit{(electric charge)} \qquad && (\epsilon \dot{\boldsymbol{E}}_h, \nabla v)_{\mathcal{T}_h} = (\nabla \cdot \boldsymbol{J}, v)_{\mathcal{T}_h}, && \text{(14a)}\\
&\textit{(magnetic charge)} \qquad && (\mu \dot{\boldsymbol{H}}_h, \nabla w)_{\mathcal{T}_h} = 0, && \text{(14b)}\\
&\textit{(energy)} \qquad && \dot{\mathcal{H}}_{w,h} = 0, && \text{(14c)}
\end{aligned}
$$

for any test functions $v, w \in H_0^1(\Omega)$ *satisfying* $(\nabla v, \nabla w) \in \mathcal{D}_h^*$.

Proof. We will only present the proof for DG method since the proofs for mixed and HDG methods are similar. To obtain the conservation of the electric charge, we define $F_{ec} = (\epsilon \boldsymbol{E}_h, \nabla v)_{\mathcal{T}_h}$ and obtain that

$$
\begin{aligned}
\dot{F}_{ec} &= \{F_{ec}, \mathcal{H}_{w,h}^{DG}\}_{w,h} = (\frac{\delta \mathcal{H}_{w,h}^{DG}}{\delta \boldsymbol{A}_h}, \nabla v)_{\mathcal{T}_h}\\
&= (\boldsymbol{H}_h, \nabla \times \nabla v)_{\mathcal{T}_h} + \langle \boldsymbol{n} \times \widehat{\boldsymbol{H}}_h, \nabla v \rangle_{\partial \mathcal{T}_h} - (\boldsymbol{J}, \nabla v)_{\mathcal{T}_h},
\end{aligned}
$$

by equation (13). By the single-valuedness of $(\nabla v)^t$ (again by [49, Lemma 3]) on $\mathcal{F}_h^0$, and since $v = 0$ on Γ, we obtain

$$
\dot{F}_{ec} = (\nabla \cdot \boldsymbol{J}, v)_{\mathcal{T}_h}.
$$

The conservation of the magnetic charge can be obtained directly from the equation giving $\boldsymbol{H}_h$ in terms of $\boldsymbol{A}_h$, (8c). Indeed, taking $\boldsymbol{r} := \nabla w$, we get

$$
(\mu \boldsymbol{H}_h, \nabla w)_{\mathcal{T}_h} = \langle \boldsymbol{n} \times \widehat{\boldsymbol{A}}_h^t, \nabla w \rangle_{\partial \mathcal{T}_h} + (\boldsymbol{A}_h, \nabla \times \nabla w)_{\mathcal{T}_h} = 0
$$

by single-valuedness of $(\nabla w)^t$ and $\widehat{\boldsymbol{A}}_h^t$, and since and $w = 0$ on Γ. Clearly, property (14b) follows naturally.

Finally, the energy conservation is obtained immediately by the antisymmetry property of the Poisson bracket $\{\cdot, \cdot\}_{w,h}$. This completes the proof.

5. Fully discrete HDG schemes

In this section, we present the time-marching Runge-Kutta, symplectic integrators with which we complete the definition of the fully discrete schemes.

5.1. Symplectic diagonally implicit Runge-Kutta methods

We discretize in time the HDG scheme using symplectic diagonally implicit Runge-Kutta (DIRK) methods. To introduce the DIRK scheme we consider the ODE $\dot{y}(t) = f(t, y(t))$. A DIRK scheme computes the approximate solution $y^{(n+1)} = y(t^{n+1})$ assuming that $y^{(n)}$ is known by

$$
y^{n+1} = y^n + \Delta t \sum_{i=1}^{s} b_i k_i,
$$

where $k_i = f(t^{n,i}, y^{n,i})$, $t^{n,i} = t^n + c_i\Delta t$, and $y^{n,i} = y^n + \Delta t \sum_{j=1}^{i} a_{ij}k_j$. The Runge-Kutta coefficient matrix a_{ij} and the coefficient vectors b_i and c_i, for $i, j = 2, .., n$, are usually summarized in a Butcher tableau. For DIRK schemes we note that $a_{ij} = 0$, for $j > i$. Furthermore, these schemes have the symplectic property under the following condition on the coefficients (see [58]):

$$b_i a_{ij} + b_j a_{ji} - b_i b_j = 0, \quad 1 \leqslant i, j \leqslant s.$$

Note that we can reduce the semidiscrete HDG scheme of the $\boldsymbol{E}$-$\boldsymbol{H}$ formulation to the following ODE system

$$\mathbb{M}\dot{\boldsymbol{y}} + \mathbb{T}\boldsymbol{y} = \mathbb{F}(t), \tag{15}$$

where $\boldsymbol{y}$ contains the degrees of freedom of $(\boldsymbol{E}_h, \boldsymbol{H}_h, \widehat{\boldsymbol{E}}_h)$. Then, to solve the system we apply an s-stages DIRK scheme. The method is shown in Algorithm 1. It is possible to perform static condensation to locally eliminate the degrees of freedom of $(\boldsymbol{E}_h, \boldsymbol{H}_h)$ to obtain a smaller linear system in terms of the degrees of freedom of $\widehat{\boldsymbol{E}}_h$.

Algorithm 1: DIRK-HDG

Data: $\boldsymbol{y}^n$
Result: $\boldsymbol{y}^{n+1}$
for $i \leftarrow 1$ **to** s **do**

$$\boldsymbol{r}_i = \frac{\boldsymbol{y}^n}{a_{ii}\Delta t} + \sum_{j=1}^{i-1} \frac{a_{ij}}{a_{ii}} \left(\frac{\boldsymbol{y}^{n,i}}{a_{ii}\Delta t} - \boldsymbol{r}_j \right);$$

Solve for $\boldsymbol{y}^{n,i}$: $\quad \mathbb{T}\boldsymbol{y}^{n,i} = \mathbb{M}\boldsymbol{r}_i + \mathbb{F}(t^n + c_i\Delta t)$;

$$k_i = \frac{\boldsymbol{y}^{n,i} - \boldsymbol{y}^n}{a_{ii}\Delta t} - \sum_{j=1}^{i-1} \frac{a_{ij}}{a_{ii}} k_j;$$

end

$$\boldsymbol{y}^{n+1} = \boldsymbol{y}^n + \Delta t \sum_{i=1}^{s} b_i k_i;$$

5.2. Symplectic explicit partitioned Runge-Kutta methods

In this section we discretize in time the HDG scheme using explicit partitioned Runge-Kutta (EPRK) methods. To introduce the EPRK scheme we consider the Hamiltonian system

$$\dot{\mathsf{p}} = -\frac{\partial \mathcal{H}}{\partial \mathsf{q}}(\mathsf{p}, \mathsf{q}, t), \quad \dot{\mathsf{q}} = \frac{\partial \mathcal{H}}{\partial \mathsf{p}}(\mathsf{p}, \mathsf{q}, t).$$

An EPRK scheme computes the approximate solution

$$(\mathsf{p}^{(n+1)}, \mathsf{q}^{(n+1)}) := (\mathsf{p}(t^{n+1}), \mathsf{q}(t^{n+1}),$$

assuming that $(\mathsf{p}(t^n), \mathsf{q}(t^n)$ is known, by using an s-stage DIRK scheme with coefficients (a_{ij}, b_i, c_i) for the first ODE and explicit RK scheme with coefficients

$(\tilde{a}_{ij}, \tilde{b}_i, \tilde{c}_i)$, for $i, j = 1, \ldots, s$ for the second equations. The global scheme is explicit if the Hamiltonian function is separable. Moreover, the scheme is symplectic if the coefficients satisfy (see [58])

$$b_i \tilde{a}_{ij} + \tilde{b}_j a_{ji} - b_i \tilde{b}_j = 0, \quad 1 \leqslant i, j \leqslant s.$$

In our case we reduce the HDG semidiscrete scheme to the following structure:

$$\mathbb{M}_1 \dot{\boldsymbol{p}} = -\mathbb{T}_1 \boldsymbol{q}, \qquad \mathbb{M}_2 \dot{\boldsymbol{q}} = \mathbb{T}_2 \boldsymbol{p} + \mathbb{F}(t) \tag{16}$$

These equation will be solved using Algorithm 2.

Algorithm 2: EPRK-HDG

Data: $(\boldsymbol{p}^{(n)}, \boldsymbol{q}^{(n)})$
Result: $(\boldsymbol{p}^{(n+1)}, \boldsymbol{q}^{(n+1)})$
$(\boldsymbol{p}_0, \boldsymbol{q}_0) \leftarrow (\boldsymbol{p}^{(n)}, \boldsymbol{q}^{(n)})$;
for $i \leftarrow 1$ **to** s **do**
  Solve for $\boldsymbol{p}_i$: $\mathbb{M}_1 \boldsymbol{p}_i = \mathbb{M}_1 \boldsymbol{p}_{i-1} - \Delta t\, b_i\, \mathbb{T}_1 \boldsymbol{q}_{i-1}$;
  Solve for $\boldsymbol{q}_i$: $\mathbb{M}_2 \boldsymbol{q}_i = \mathbb{M}_2 \boldsymbol{q}_{i-1} - \Delta t \tilde{b}_i \left(\mathbb{T}_2 \boldsymbol{p}_i + \mathbb{F}(t + \tilde{c}_i)\right)$;
end
$(\boldsymbol{p}^{(n+1)}, \boldsymbol{q}^{(n+1)}) \leftarrow (\boldsymbol{p}_s, \boldsymbol{q}_s)$;

5.3. Fully discrete HDG schemes for the electric and magnetic vector potential formulation.

We rewrite the HDG scheme (8)-(9) as: Find $(\boldsymbol{A}_h, \boldsymbol{E}_h, \boldsymbol{H}_h, \widehat{\boldsymbol{A}}_h^t) \in V_h \times V_h \times W_h \times M_h^t$

$$\begin{aligned}
(\epsilon \dot{\boldsymbol{A}}_h, \boldsymbol{v}_h)_{\mathcal{T}_h} + (\epsilon \boldsymbol{E}, \boldsymbol{v}_h)_{\mathcal{T}_h} &= 0\\
(\epsilon\, \dot{\boldsymbol{E}}_h, \boldsymbol{v}_h)_{\mathcal{T}_h} - (\nabla \times \boldsymbol{H}_h, \boldsymbol{v}_h)_{\mathcal{T}_h} - \langle \tau_t (P_M \boldsymbol{A}_h - \widehat{\boldsymbol{A}}_h) \times \boldsymbol{n}, \boldsymbol{v}_h \times \boldsymbol{n} \rangle_{\partial \mathcal{T}_h} &= (\boldsymbol{J}, \boldsymbol{v}_h)_{\mathcal{T}_h}\\
(\mu \boldsymbol{H}_h, \boldsymbol{w}_h)_{\mathcal{T}_h} - \langle \boldsymbol{n} \times \widehat{\boldsymbol{A}}_h^t, \boldsymbol{w}_h \rangle_{\partial \mathcal{T}_h} - (\boldsymbol{A}_h, \nabla \times \boldsymbol{w}_h)_{\mathcal{T}_h} &= 0\\
\langle \boldsymbol{n} \times (\boldsymbol{H}_h^t + \tau P_M (\boldsymbol{A}_h - \widehat{\boldsymbol{A}}_h)), \boldsymbol{\eta}_h \rangle_{\partial \mathcal{T}_h} &= 0\\
\langle \boldsymbol{n} \times \widehat{\boldsymbol{A}}_h^t, \boldsymbol{\eta}_h \rangle_{\Gamma} &= \langle \boldsymbol{g}_{\boldsymbol{A}}, \boldsymbol{\eta} \rangle_{\Gamma}
\end{aligned}$$

for all $(\boldsymbol{v}_h, \boldsymbol{v}_h, \boldsymbol{w}_h, \boldsymbol{\eta}_h) \in V_h \times V_h \times W_h \times M_h^t$.

To obtain the fully discrete implicit scheme using symplectic DIRK methods, we note that the HDG scheme has the structure (15) with $\boldsymbol{y}$ being the degrees of freedom of $(\boldsymbol{A}_h, \boldsymbol{E}_h, \boldsymbol{H}_h, \widehat{\boldsymbol{A}}_h^t)$. Furthermore, the matrix $\mathbb{M}$ is block diagonal, and since there is no time derivative for $\boldsymbol{H}_h$ and $\widehat{\boldsymbol{A}}_h^t$ then the corresponding blocks to these unknowns are zero.

To obtain the fully discrete explicit scheme using symplectic EPRK time integrators, we write the HDG scheme in the form (16). The variables $\boldsymbol{p}$ and $\boldsymbol{q}$ correspond to the coefficients of the approximations of $\boldsymbol{A}_h$ and $\boldsymbol{E}_h$. We observe that in the second equation of the HDG scheme we need to write the variables $\boldsymbol{H}_h$ and $\widehat{\boldsymbol{A}}_h^t$ in terms of the variable $\boldsymbol{A}_h$. For this purpose we use the third and fourth equations and obtain the system for a given $\boldsymbol{A}_h$, find $(\boldsymbol{H}_h, \widehat{\boldsymbol{A}}_h^t) \in W_h \times M_h^t$ such that

$$\begin{aligned}
(\mu \boldsymbol{H}_h, \boldsymbol{r}_h)_{\mathcal{T}_h} - \langle \boldsymbol{n} \times \widehat{\boldsymbol{A}}_h^t, \boldsymbol{r}_h \rangle_{\partial \mathcal{T}_h} &= -(\boldsymbol{A}_h, \nabla \times \boldsymbol{r}_h)_{\mathcal{T}_h} \\
\langle \boldsymbol{H}_h^t - \tau \widehat{\boldsymbol{A}}_h \times \boldsymbol{n}, \boldsymbol{\eta}_h \times \boldsymbol{n} \rangle_{\partial \mathcal{T}_h} &= \langle \tau P_M \boldsymbol{A}_h \times \boldsymbol{n}, \boldsymbol{\eta}_h \times \boldsymbol{n} \rangle_{\partial \mathcal{T}_h} \\
\langle \boldsymbol{n} \times \widehat{\boldsymbol{A}}_h^t, \boldsymbol{\eta}_h \rangle_{\Gamma} &= \langle \boldsymbol{g}_{\boldsymbol{A}}, \boldsymbol{\eta}_h \rangle_{\Gamma}
\end{aligned}$$

for all $(\boldsymbol{w}_h, \boldsymbol{\eta}_h) \in W_h \times M_h^t$.

6. Numerical experiments

In this section, we test the properties of our numerical schemes, specifically the EPRK$(k+2)$-HDG$_k(\mathfrak{B})$ (variant $\mathfrak{B}$, third HDG method in Table 5, see also Remark 3.1) and DIRK$(k+1)$-HDG$_k$ (variant k, first HDG method in Table 5, see also Remark 3.1) numerical schemes. We use an EPRK method of order $(k+2)$ when we use the HDG method with variant $\mathfrak{B}$, i.e. matching the expected rate of convergence of the error of the electric field and the magnetic vector potential. We use a DIRK method of order $(k+1)$ when we use the HDG method with variant k with polynomial order k, again matching the expected rate of convergence of the error of the variables. For all numerical experiments we use the open source finite element library NETGEN [59] and NGSolve [60].

In Section 6.1, we provide numerical evidence of the approximation properties of the EPRK$(k+2)$-HDG$_k(\mathfrak{B})$ method obtaining the optimal convergence of order $k+2$ for the L^2-errors of the electric field and the magnetic vector potential variables and of order $k+1$ for the L^2-errors of the magnetic field. In Section 6.2, we present a numerical example illustrating the energy-conserving property of our methods, in particular we use DIRK$(k+1)$-HDG$_k$ (variant k), with $k=1$. Note that the symplectic Runge-Kutta schemes integrates exactly quadratic forms. This is observed in our experiment.

6.1. Convergence tests

In the following numerical experiment, we provide evidence of the optimal approximation properties of the numerical scheme EPRK$(k+2)$-HDG$_k$ (variant $\mathcal{B}$). See Appendix G for the EPRK schemes used in our computations. For each of the approximations $\boldsymbol{E}_h$, $\boldsymbol{A}_h$, and $\boldsymbol{H}_h$, we compute the maximum over the time steps t^n of the L^2-errors of the corresponding error, and then estimate their orders of convergence (e.o.c.). For instance, for the electric field approximation we compute

$$\text{error}(h) = \max_{t^n} \|\boldsymbol{E}(t^n) - \boldsymbol{E}_h^n\|_{L^2(\Omega)^3}, \qquad \text{e.o.c}(h) = \frac{\log(\text{error}_h/\text{error}_{h'})}{\log(h/h')},$$

where h' correspond to the previous mesh size parameter used in the computations. The experiment is carried on the unit cubic domain $\Omega = (0,1)^3$ using uniform triangulations with mesh-size parameter $h = 2^{-l}$. As exact solution of the initial, boundary-value problem (1), consider the example from [15] given by

$$
\begin{aligned}
\boldsymbol{E}(x,y,z) &= \begin{pmatrix} -\cos(\pi x)\sin(\pi y)\sin(\pi z)\cos(\omega t) \\ 0 \\ \sin(\pi x)\sin(\pi y)\cos(\pi z)\cos(\omega t) \end{pmatrix}, \\
\boldsymbol{H}(x,y,z) &= \begin{pmatrix} -\frac{\pi}{\omega}\sin(\pi x)\cos(\pi y)\cos(\pi z)\sin(\omega t) \\ \frac{2\pi}{\omega}\cos(\pi x)\sin(\pi y)\cos(\pi z)\sin(\omega t) \\ -\frac{\pi}{\omega}\cos(\pi x)\cos(\pi y)\sin(\pi z)\sin(\omega t) \end{pmatrix}
\end{aligned}
$$

with angular frequency $\omega = \sqrt{3}\pi$ and with permittivity and permeability $\epsilon = 1$ and $\mu = 1$.

We show in Table 6 the errors and orders of convergence for the EPRK(k+2)-HDG$_k$($\mathfrak{B}$) method. We observe the optimal convergence in L^2 norm of order $k+2$ ~~for the L^2-errors of~~ for the electric field and the magnetic vector potential variables, and of order $k+1$ for the magnetic field.

Table 6: History of convergence of the numerical approximations of Maxwell's equations (2) by semidiscrete HDG scheme (8) variant $\mathfrak{B}$ with ESPRK($k+2$).

		$\boldsymbol{E}_h$		$\boldsymbol{A}_h$		$\boldsymbol{H}_h$	
k	h	error	e.o.c.	error	e.o.c.	error	e.o.c.
0	7.9370e-01	2.9675e-01	–	6.8615e-02	–	4.1701e-01	–
	3.9685e-01	1.1164e-01	1.41	2.1249e-02	1.69	2.5653e-01	0.70
	1.9843e-01	2.6226e-02	2.08	5.1184e-03	2.05	1.2883e-01	0.99
	9.9213e-02	7.4169e-03	1.82	1.3227e-03	1.95	6.4956e-02	0.98
	4.9606e-02	1.9690e-03	1.91	3.3288e-04	1.99	3.2532e-02	0.99
1	7.9370e-01	6.4480e-02	–	9.7970e-03	–	1.4015e-01	–
	3.9685e-01	1.6202e-02	1.99	2.7083e-03	1.85	5.8194e-02	1.26
	1.9843e-01	2.5722e-03	2.65	3.4638e-04	2.96	1.7300e-02	1.75
	9.9213e-02	3.4336e-04	2.90	4.4523e-05	2.95	4.4140e-03	1.97
2	7.9370e-01	3.5762e-02	–	6.5098e-03	–	4.0838e-02	–
	3.9685e-01	3.2224e-03	3.47	5.7848e-04	3.49	7.9169e-03	2.36
	1.9843e-01	2.1460e-04	3.90	3.4372e-05	4.07	9.2374e-04	3.09
	9.9213e-02	1.4210e-05	3.91	2.1960e-06	3.96	1.1636e-04	2.98
3	7.9370e-01	3.0788e-03	–	5.4199e-04	–	1.2561e-02	–
	3.9685e-01	3.8432e-04	3.00	6.6832e-05	3.01	1.8175e-03	2.78
	1.9843e-01	1.9462e-05	4.30	2.9721e-06	4.49	1.5816e-04	3.52
	9.9213e-02	6.4882e-07	4.90	9.5185e-08	4.96	1.0231e-05	3.95

6.2. Conservation properties

To test the conservation properties of our schemes under consideration, we consider a monochromatic (single frequency) plane wave traveling in the vacuum, in which case $\boldsymbol{J} = 0$, $\rho = 0$, and the electric and magnetic permeability are constant. The plane wave solution has the following general form:

$$
\boldsymbol{E} = \boldsymbol{E}_0 e^{i(\boldsymbol{k}\cdot\boldsymbol{x} - \omega t)}, \quad \boldsymbol{H} = \boldsymbol{H}_0 e^{i(\boldsymbol{k}\cdot\boldsymbol{x} - \omega t)},
$$

where $\boldsymbol{E}_0$ and $\boldsymbol{H}_0$ are constant amplitudes which can take complex values, and the angular frequency ω and the wavenumber $\boldsymbol{k}$ satisfy $\epsilon_0\mu_0 = \frac{|\boldsymbol{k}|^2}{\omega^2}$. The plane wave is a solution of the Maxwell's equations if and only if

$$-\omega\epsilon_0 \boldsymbol{E}_0 = \boldsymbol{k} \times \boldsymbol{H}_0, \quad \omega\mu_0 \boldsymbol{H}_0 = \boldsymbol{k} \times \boldsymbol{E}_0, \quad \boldsymbol{k} \cdot \boldsymbol{H}_0 = 0, \quad \boldsymbol{k} \cdot \boldsymbol{E}_0 = 0.$$

For $\boldsymbol{k} = (\kappa, 0, 0)$, $\boldsymbol{H}_0 = (0, H_0, 0)$ and $\boldsymbol{x} := (x, y, z)$, we have a plane wave solution traveling along the x-axis:

$$\boldsymbol{k} = (\kappa, 0, 0)^\top, \ \boldsymbol{E} = (0, 0, \frac{-\kappa H_0}{\omega\epsilon_0})^\top \sin(\kappa x - \omega t), \ \boldsymbol{H} = (0, H_0, 0)^\top \sin(\kappa x - \omega t).$$

In our computations, we consider a cubic domain $(0, 2) \times (0, 1) \times (0, 1)$ with periodic boundary conditions, and $\kappa = \omega = 2$. We compute using the scheme HDG_1, i.e., polynomial spaces of degree $k = 1$ for all the variables, and as a symplectic numerical integrator we use the implicit-midpoint or DIRK(2).

In Fig. 2, we plot the approximate energy, optical chirality, the first component of the linear momentum, the second component of the angular momentum, the electric charge and the magnetic charge, for a sequence of three triangulations with mesh-size parameters given by $h, h/2, h/4$, starting with $h = 0.25$. We observe the exact conservation of the energy for the three meshes and the fast convergence to the exact energy. We also observe that the electric and magnetic charges oscillate around zero and that the oscillations are extremely small and less than 10^{-13}.

As for the quadratic functionals of optical chirality, linear and angular electromagnetic momenta, we see that they remain remarkably no-drifting and with oscillations which decrease in amplitude as the mesh is refined. Theoretical computations for the total electromagnetic linear momentum, not reported here, show that, when the continuous version is supposed to remain constant, its discrete version varies in time as a quadratic function of the jumps of the approximate solution. This might explain that its order of convergence is at least $2k$. We expect a similar behavior for the remaining quadratic functionals on Table 2, but more work needs to be done to understand their convergence properties.

7. Extensions

In this Section, we describe the modifications that have to be made when working with other boundary conditions, and with other weak formulations of the Maxwell's equations.

7.1. Other boundary conditions

Here, we sketch how to extend our results when the boundary condition is

$$\boldsymbol{n} \times \boldsymbol{H} = \boldsymbol{g}_H \quad \text{on } \Gamma.$$

We consider the case of the $\boldsymbol{E}$-$\boldsymbol{A}$ formulation, as it is particularly simple and illustrative.

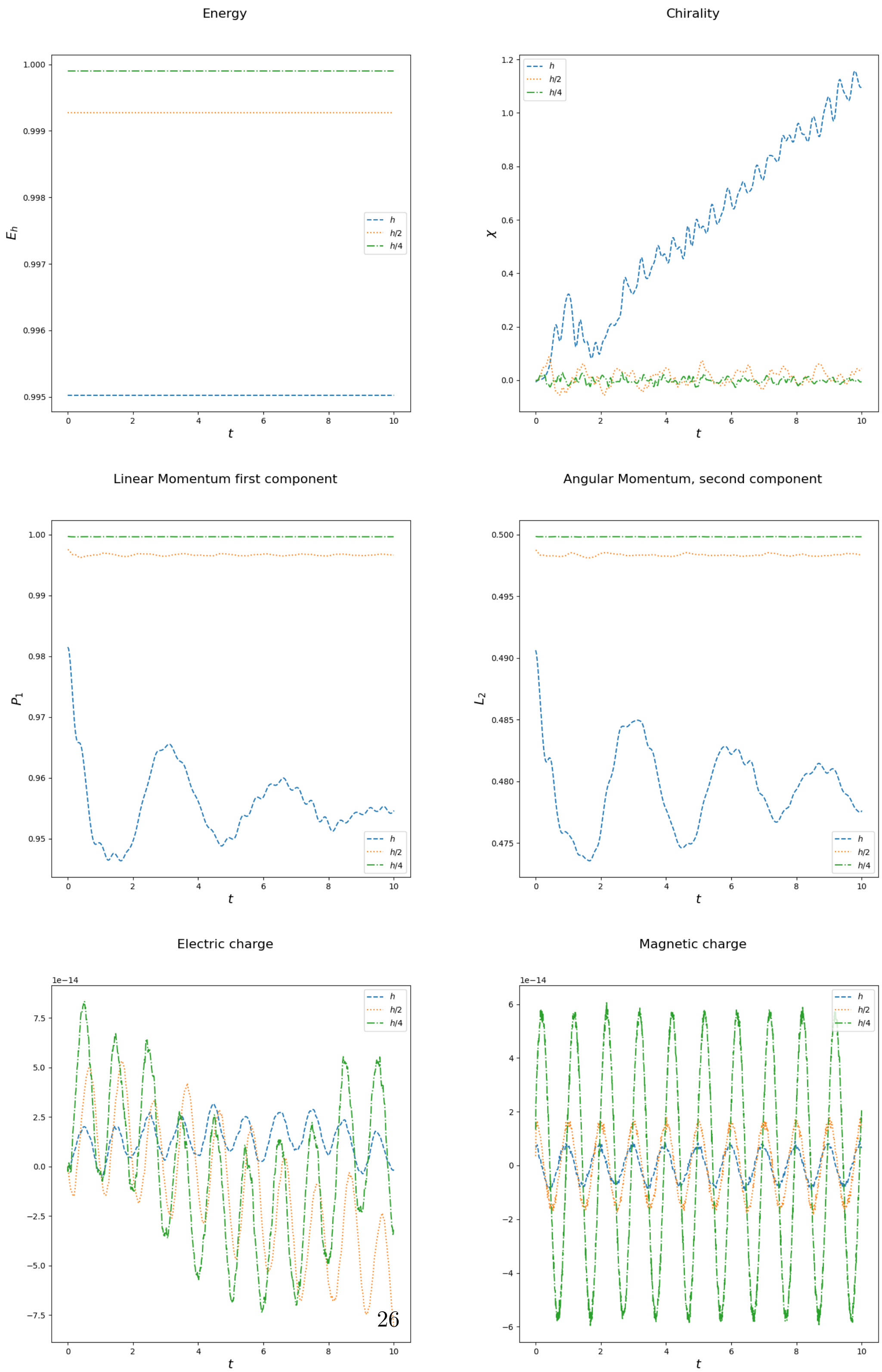

Figure 2: Electromagnetic energy (top, left), optical chirality (top, right), first component of the electromagnetic linear momentum (middle, left), second component of the electromagnetic angular momentum (middle, left) electric charge (bottom, left), and magnetic charge (bottom, right).

First, as it is standard for the mixed method, we incorporate the boundary condition for $\boldsymbol{H}$ into the corresponding space. So, we take $\boldsymbol{H}$ as the element of $\mathbf{H}(\mathrm{curl}, \Omega; \mathrm{g_H})$ such that

$$\int_\Omega \mu\, \boldsymbol{H} \cdot \boldsymbol{\psi} = \int_\Omega \boldsymbol{A} \cdot \nabla \times \boldsymbol{\psi} \qquad \forall\, \boldsymbol{\psi} \in \mathbf{H}(\mathrm{curl}, \Omega; 0).$$

Since there are no boundary conditions on $\boldsymbol{A}$, the smooth manifold $\mathcal{M}$ and test functions space $\mathcal{T}$ are now

$$\begin{aligned} \mathcal{M} &= \boldsymbol{L}^2(\Omega) \times \boldsymbol{L}^2(\Omega), \\ \mathcal{D} &= \mathcal{C}^\infty(\Omega) \times \mathcal{C}^\infty(\Omega). \end{aligned}$$

Finally, a term capturing the new boundary conditions needs to be added to the Hamiltonian. In this case, the Hamiltonian is

$$\mathcal{H}_w(\boldsymbol{E}, \boldsymbol{A}) \;=\; \frac{1}{2} \int_\Omega \big(\epsilon \boldsymbol{E} \cdot \boldsymbol{E} + \mu \boldsymbol{H} \cdot \boldsymbol{H}\big) - \int_\Omega \boldsymbol{A} \cdot \boldsymbol{J} - \int_\Gamma \boldsymbol{A} \cdot \boldsymbol{g_H}.$$

The Poisson bracket and the coordinate functionals remain unchanged. With these modifications, it can be easily shown that $(\mathcal{M}, \{\cdot,\cdot\}_w, \mathcal{H}_w)$ is a Hamiltonian dynamical system defined by the $\boldsymbol{E}$-$\boldsymbol{A}$ formulation.

Now, let us describe the changes we need to make to the numerical schemes. First, we describe the changes to be made to the definition of the schemes. For the mixed method, we take $(\boldsymbol{E}_h, \boldsymbol{A}_h, \boldsymbol{H}_h)$ in the space $\boldsymbol{V}_h \times \boldsymbol{V}_h \times \boldsymbol{W}_h^{\mathrm{curl}}(\boldsymbol{g_H})$ and take the corresponding test functions in $\boldsymbol{V}_h \times \boldsymbol{V}_h \times \boldsymbol{W}_h^{\mathrm{curl}}(\mathbf{0})$. In particular, note that the equation defining $\boldsymbol{H}_h$ in terms of $\boldsymbol{A}_h$ now reads:

$$(\mu \boldsymbol{H}_h, \boldsymbol{r})_{\mathcal{T}_h} + (\boldsymbol{A}_h, \nabla \times \boldsymbol{r})_{\mathcal{T}_h} + \langle \boldsymbol{n} \times \widehat{\boldsymbol{A}}_h, \boldsymbol{r} \rangle_{\partial \mathcal{T}_h} = 0 \quad \forall \boldsymbol{r} \in \boldsymbol{W}_h^{\mathrm{curl}}(\mathbf{0}). \tag{17}$$

For the HDG and DG methods, there are no changes to their weak formulations. Only their numerical traces have to change to capture the new boundary conditions, see Table 7.

Table 7: Numerical traces.

method		$\boldsymbol{E}$-$\boldsymbol{A}$ formulation
HDG	on $\mathcal{F}_h^\partial$:	$\boldsymbol{n} \times \widehat{\boldsymbol{H}}_h = \boldsymbol{g_H}$
		$\widehat{\boldsymbol{A}}_h \in \boldsymbol{M}_h$ is a new unknown:
	on $\partial \mathcal{T}_h$:	$\boldsymbol{n} \times (\widehat{\boldsymbol{H}}_h - \boldsymbol{H}_h) = \tau(\boldsymbol{P_M} \boldsymbol{A}_h - \widehat{\boldsymbol{A}}_h)$
DG	on $\mathcal{F}_h^0$:	$\widehat{\boldsymbol{H}}_h = \{\!\{\boldsymbol{H}_h\}\!\} - C_{11} [\![\boldsymbol{A}_h]\!] + \underline{\boldsymbol{C}}_{12}^T [\![\boldsymbol{H}_h]\!]$
		$\widehat{\boldsymbol{A}}_h = \{\!\{\boldsymbol{A}_h\}\!\} + \underline{\boldsymbol{C}}_{12} [\![\boldsymbol{A}_h]\!] + C_{22}\, [\![\boldsymbol{H}_h]\!]$
	on $\mathcal{F}_h^\partial$:	$\boldsymbol{n} \times \widehat{\boldsymbol{H}}_h = \boldsymbol{g_H}$
		$\widehat{\boldsymbol{A}}_h = \boldsymbol{A}_h + C_{22}\, \boldsymbol{n} \times (\boldsymbol{H}_h - \widehat{\boldsymbol{H}}_h)$

Next, we consider the changes to be made to the components of the Hamiltonian structure. Again, since there are no boundary conditions on $\boldsymbol{A}$, the smooth manifold $\mathcal{M}$ and test functions space $\mathcal{T}$ are

$$\begin{aligned}\mathcal{M} &= \boldsymbol{V}_h \times \boldsymbol{V}_h,\\ \mathcal{D} &= \boldsymbol{V}_h \times \boldsymbol{V}_h.\end{aligned}$$

As in the continuous case, a term capturing the new boundary conditions needs to be added to the Hamiltonian which becomes

$$\begin{aligned}\mathcal{H}^*_{w,h} =& \frac{1}{2}\left((\epsilon \boldsymbol{E}_h, \boldsymbol{E}_h)_{\mathcal{T}_h} + (\mu \boldsymbol{H}_h, \boldsymbol{H}_h)_{\mathcal{T}_h} + \langle \boldsymbol{n} \times (\widehat{\boldsymbol{H}}^*_h - \boldsymbol{H}_h), \boldsymbol{A}_h - \widehat{\boldsymbol{A}}^*_h \rangle_{\partial \mathcal{T}_h}\right)\\ &- (\boldsymbol{A}_h, \boldsymbol{J})_{\mathcal{T}_h} - \langle \widehat{\boldsymbol{A}}^*_h, \boldsymbol{g}_{\boldsymbol{H}} \rangle_{\Gamma},\end{aligned}$$

where the numerical trace $\widehat{\boldsymbol{A}}^*_h$ needs to be defined on Γ for the mixed method. We take it as the element of

$$\{\boldsymbol{n} \times \boldsymbol{w}|_{\Gamma} :\ \boldsymbol{w} \in \boldsymbol{W}_h^{\text{curl}}\}$$

which solves

$$\langle \widehat{\boldsymbol{A}}^M_h, \boldsymbol{n} \times \boldsymbol{r} \rangle_{\partial \mathcal{T}_h} = -(\mu \boldsymbol{H}_h, \boldsymbol{r})_{\mathcal{T}_h} + (\boldsymbol{A}_h, \nabla \times \boldsymbol{r})_{\mathcal{T}_h} \quad \forall \boldsymbol{r} \in \boldsymbol{W}_h^{\text{curl}}.$$

The auxiliary numerical trace $\widehat{\boldsymbol{A}}^M_h$ is well defined thanks to the weak formulation (17) defining $\boldsymbol{H}_h$ as a function of $\boldsymbol{A}_h$.

Finally, the Poisson bracket and the coordinate functionals remain unchanged. With these modifications, it can be easily shown that Theorem 4.2 and Corollary 4.2 do hold.

7.2. Other weak formulations

Since the roles of the electric and the magnetic field in the Maxwell's equations can be considered to be fairly symmetric, one could easily argue that it is natural to switch them. Here, we show how to do that for the $\boldsymbol{E}$-$\boldsymbol{H}$ formulation. We are going to switch the spaces, but are going to keep the boundary condition unchanged.

So, in this case, the phase manifold and the space of test functions are

$$\begin{aligned}\mathcal{M} &= \mathbf{H}(\text{curl}, \Omega; \text{g}_{\text{E}}) \times \boldsymbol{L}^2(\Omega),\\ \mathcal{D} &= \mathcal{C}^\infty(\Omega; \mathbf{0}) \qquad \times \mathcal{C}^\infty(\Omega),\end{aligned}$$

and the Poisson bracket is

$$\{F, G\}_{\mathcal{E}} \;=\; \int_\Omega \left(\nabla \times \left(\frac{1}{\epsilon}\frac{\delta F}{\delta \boldsymbol{E}}\right) \cdot \left(\frac{1}{\mu}\frac{\delta G}{\delta \boldsymbol{H}}\right) - \nabla \times \left(\frac{1}{\epsilon}\frac{\delta G}{\delta \boldsymbol{E}}\right) \cdot \left(\frac{1}{\mu}\frac{\delta F}{\delta \boldsymbol{H}}\right)\right).$$

The Hamiltonian and coordinate functionals remain unchanged. A simple computation shows that $(\mathcal{M}, \{\cdot,\cdot\}_w, \mathcal{H}_w)$ is a Hamiltonian dynamical system defined by the $\boldsymbol{E}$-$\boldsymbol{H}$ formulation.

Indeed, if we take the following coordinate functionals

$$F_{\boldsymbol{E}}(\boldsymbol{\phi}) = \int_\Omega \epsilon\, \boldsymbol{E}\cdot\boldsymbol{\phi}, \quad F_{\boldsymbol{H}}(\boldsymbol{\psi}) = \int_\Omega \mu\, \boldsymbol{H}\cdot\boldsymbol{\psi},$$

we have that

$$\frac{1}{\epsilon}\frac{\delta F_{\boldsymbol{E}}}{\delta \boldsymbol{E}} = \boldsymbol{\phi}, \quad \frac{1}{\mu}\frac{\delta F_{\boldsymbol{E}}}{\delta \boldsymbol{H}} = 0, \quad \frac{1}{\epsilon}\frac{\delta F_{\boldsymbol{H}}}{\delta \boldsymbol{E}} = 0, \quad \frac{1}{\mu}\frac{\delta F_{\boldsymbol{H}}}{\delta \boldsymbol{H}} = \boldsymbol{\psi},$$

and since

$$\frac{1}{\epsilon}\frac{\delta \mathcal{H}_{\mathcal{E}}}{\delta \boldsymbol{E}} = \boldsymbol{E}, \quad \frac{1}{\mu}\frac{\delta \mathcal{H}_{\mathcal{E}}}{\delta \boldsymbol{H}} = \boldsymbol{H} - \boldsymbol{J}_\times,$$

we get

$$\begin{aligned}
\int_\Omega \epsilon\, \dot{\boldsymbol{E}}\cdot\boldsymbol{\phi} = \dot{F}_{\boldsymbol{E}} = \{F_{\boldsymbol{E}}, \mathcal{H}_{\mathcal{E}}\}_{\mathcal{E}} &= \int_\Omega \nabla\times\boldsymbol{\phi}\cdot(\boldsymbol{H}-\boldsymbol{J}_\times) = \int_\Omega (\nabla\times\boldsymbol{H}-\boldsymbol{J})\cdot\boldsymbol{\phi},\\
\int_\Omega \mu\, \dot{\boldsymbol{H}}\cdot\boldsymbol{\psi} = \dot{F}_{\boldsymbol{H}} = \{F_{\boldsymbol{H}}, \mathcal{H}_{\mathcal{E}}\}_{\mathcal{E}} &= -\int_\Omega \nabla\times\boldsymbol{E}\cdot\boldsymbol{\psi},
\end{aligned}$$

for all $(\boldsymbol{\phi}, \boldsymbol{\psi})$ test functions in $\mathcal{D}$. Thus, we get a weak formulation of the first two and the fifth of equations (1). This proves our claim. Note that the weak formulation we get is different from the one obtained originally.

Let us now describe how to modify the numerical schemes. For the mixed method, there are a few changes. First, we have to use the real trace instead of the exterior trace. Then, we have to take the approximation $(\boldsymbol{E}_h, \boldsymbol{H}_h)$ in $\boldsymbol{V}_h^{\mathrm{curl}}(\boldsymbol{g}_{\boldsymbol{E}}) \times \boldsymbol{W}_h$ and is required to satisfy the equations

$$\begin{aligned}
(\epsilon\, \dot{\boldsymbol{E}}_h, \boldsymbol{v})_{\mathcal{T}_h} - (\boldsymbol{H}_h, \nabla\times\boldsymbol{v})_{\mathcal{T}_h} &= -(\boldsymbol{J}, \boldsymbol{v})_{\mathcal{T}_h} \qquad && \forall \boldsymbol{v}\in \boldsymbol{V}_h^{\mathrm{curl}}(\boldsymbol{0}),\\
(\mu\, \dot{\boldsymbol{H}}_h, \boldsymbol{r})_{\mathcal{T}_h} + (\nabla\times\boldsymbol{E}_h, \boldsymbol{r})_{\mathcal{T}_h} &= 0 && \forall \boldsymbol{r}\in \boldsymbol{W}_h.
\end{aligned}$$

In Table 8, we show two examples of mixed methods of the type just described. The superscript "div" indicates that the space is a subspace of $\boldsymbol{H}(\mathrm{div}, \Omega)$. This is not necessary, as the weak formulation only requires $\boldsymbol{W}_h$ to be a subspace of $\boldsymbol{L}^2(\Omega)$.

For the DG and HDG methods, no changes need to be carried out. To end,

Table 8: Examples finite dimensional spaces for mixed methods.

	K	$\boldsymbol{V}(K)$	$\boldsymbol{W}(K)$	k	global spaces
[40, 48]	tetrahedron	$\boldsymbol{\mathcal{P}}_k \oplus (\boldsymbol{x}\times\widetilde{\boldsymbol{\mathcal{P}}}_k)$	$\boldsymbol{\mathcal{P}}_k \oplus \boldsymbol{x}\widetilde{\mathcal{P}}_k$	$\geqslant 0$	$\boldsymbol{V}_h^{\mathrm{curl}} \times \boldsymbol{W}_h^{\mathrm{div}}$
[49]	tetrahedron	$\boldsymbol{\mathcal{P}}_{k+1}$	$\boldsymbol{\mathcal{P}}_k$	$\geqslant 1$	$\boldsymbol{V}_h^{\mathrm{curl}} \times \boldsymbol{W}_h^{\mathrm{div}}$

let us describe the changes to the components of the Hamiltonian structure of the numerical methods. In fact, the only thing that changes are the space associate with the mixed methods. They are

$$\mathcal{M}_h^M := \boldsymbol{V}^{\text{curl}}(\boldsymbol{g_E}) \times \boldsymbol{W}_h \quad \text{ and } \quad \mathcal{D}_h^M := \boldsymbol{V}^{\text{curl}}(\boldsymbol{0}) \times \boldsymbol{W}_h.$$

It is not difficult to verify that Theorem 4.1 and Corollary Appendix C do hold for these new methods.

We end by noting that the introduction of SH finite element methods for nonlinear Hamiltonian systems modeling physical phenomena of practical interest constitutes the subject of ongoing work.

Appendix A. Numerical traces of HDG methods

Here we show how to write the numerical traces of HDG methods in a classic DG format. Consider the case that $\widehat{\boldsymbol{E}}_h$ is the hybrid unknown. Then $\boldsymbol{n} \times \widehat{\boldsymbol{H}}_h := \boldsymbol{n} \times \boldsymbol{H}_h - \tau \boldsymbol{P}_M(\boldsymbol{E}_h - \widehat{\boldsymbol{E}}_h)$. If we let $F \in \mathcal{E}_h^0$ be an interior face and denote the restriction from the two sides of this face by the superscripts $+/-$, see Fig. 1, then, on the face F, we can write that

$$\begin{aligned} \boldsymbol{n}^+ \times \widehat{\boldsymbol{H}}_h &= \boldsymbol{n}^+ \times \boldsymbol{H}_h^+ - \tau^+(\boldsymbol{P}_M \boldsymbol{E}_h^+ - \widehat{\boldsymbol{E}}_h), \\ \boldsymbol{n}^- \times \widehat{\boldsymbol{H}}_h &= \boldsymbol{n}^- \times \boldsymbol{H}_h^- - \tau^-(\boldsymbol{P}_M \boldsymbol{E}_h^- - \widehat{\boldsymbol{E}}_h). \end{aligned}$$

Adding these equations, we obtain

$$\widehat{\boldsymbol{E}}_h = \frac{\tau^+}{\tau^+ + \tau^-} \boldsymbol{P}_M \boldsymbol{E}_h^+ + \frac{\tau^-}{\tau^+ + \tau^-} \boldsymbol{P}_M \boldsymbol{E}_h^- - \frac{1}{\tau^+ + \tau^-} [\![\boldsymbol{H}_h]\!],$$

and inserting this expression into any of the the above expressions for $\widehat{\boldsymbol{H}}_h$, we get

$$\begin{aligned} \widehat{\boldsymbol{H}}_h =& \frac{\frac{1}{\tau^+}}{(\frac{1}{\tau^+} + \frac{1}{\tau^-})} (\boldsymbol{H}_h^+)^t + \frac{\frac{1}{\tau^-}}{(\frac{1}{\tau^+} + \frac{1}{\tau^-})} (\boldsymbol{H}_h^-)^t + \frac{1}{(\frac{1}{\tau^+} + \frac{1}{\tau^-})} [\![\boldsymbol{P}_M \boldsymbol{E}_h]\!] \\ =& \frac{\tau^-}{\tau^+ + \tau^-} (\boldsymbol{H}_h^+)^t + \frac{\tau^+}{\tau^+ + \tau^-} (\boldsymbol{H}_h^-)^t + \frac{\tau^+ \tau^-}{\tau^+ + \tau^-} [\![\boldsymbol{P}_M \boldsymbol{E}_h]\!]. \end{aligned}$$

Appendix B. Proof of Theorem

To prove this theorem, we are going to use the following auxiliary result. Its proof can be found in Appendix D.

Lemma Appendix B.1. *For any vector-valued functions* $\boldsymbol{a}$ *and* $\boldsymbol{b}$ *in* $\boldsymbol{L}^2(\partial \mathcal{T}_h)$, *we have*

$$\langle \boldsymbol{n} \times \boldsymbol{a}, \boldsymbol{b} \rangle_{\partial \mathcal{T}_h} = \langle [\![\boldsymbol{a}]\!], \{\!\{\boldsymbol{b}\}\!\} \rangle_{\mathcal{F}_h^0} - \langle \{\!\{\boldsymbol{a}\}\!\}, [\![\boldsymbol{b}]\!] \rangle_{\mathcal{F}_h^0} + \langle \boldsymbol{n} \times \boldsymbol{a}, \boldsymbol{b} \rangle_{\Gamma}.$$

We are now ready to prove Theorem 4.1.

Proof. We prove the result for the DG method. The proof for the mixed and HDG methods is similar. By definition of the coordinate functionals $F_{\boldsymbol{E}_h}$ and $F_{\boldsymbol{H}_h}$, we have that

$$\frac{1}{\epsilon}\frac{\delta F_{\boldsymbol{E}_h}}{\delta \boldsymbol{E}_h} = \boldsymbol{v}, \quad \frac{1}{\mu}\frac{\delta F_{\boldsymbol{E}_h}}{\delta \boldsymbol{H}_h} = 0, \quad \frac{1}{\epsilon}\frac{\delta F_{\boldsymbol{H}_h}}{\delta \boldsymbol{E}_h} = 0, \quad \frac{1}{\mu}\frac{\delta F_{\boldsymbol{H}_h}}{\delta \boldsymbol{H}_h} = \boldsymbol{r},$$

and, by definition of the Hamiltonian $\mathcal{H}_{\mathcal{E},h}$, we have that

$$\frac{1}{\epsilon}\frac{\delta \mathcal{H}_{\mathcal{E},h}}{\delta \boldsymbol{E}_h} = \boldsymbol{E}_h, \quad \frac{1}{\mu}\frac{\delta \mathcal{H}_{\mathcal{E},h}}{\delta \boldsymbol{H}_h} = \boldsymbol{H}_h - \boldsymbol{J}_\times.$$

Therefore,

$$\begin{aligned} (\epsilon\, \dot{\boldsymbol{E}}_h, \boldsymbol{v})_{\mathcal{T}_h} &= \dot{F}_{\boldsymbol{E}_h} = \{F_{\boldsymbol{E}_h}, \mathcal{H}_{\mathcal{E},h}\}_{\mathcal{E},h} = \Theta_{\boldsymbol{E}_h}, \\ (\mu\, \dot{\boldsymbol{H}}_h, \boldsymbol{r})_{\mathcal{T}_h} &= \dot{F}_{\boldsymbol{H}_h} = \{F_{\boldsymbol{H}_h}, \mathcal{H}_{\mathcal{E},h}\}_{\mathcal{E},h} = \Theta_{\boldsymbol{H}_h}, \end{aligned}$$

where

$$\begin{aligned} \Theta_{\boldsymbol{E}_h} &:= (\boldsymbol{v}, \nabla \times (\boldsymbol{H}_h - \boldsymbol{J}_\times))_{\mathcal{T}_h} + \langle \boldsymbol{n} \times \check{\boldsymbol{v}}, \boldsymbol{H}_h - \boldsymbol{J}_\times \rangle_{\partial\mathcal{T}_h}, \\ \Theta_{\boldsymbol{H}_h} &:= -\,(\boldsymbol{E}_h, \nabla \times \boldsymbol{r})_{\mathcal{T}_h} - \langle \boldsymbol{n} \times \check{\boldsymbol{E}}_h, \boldsymbol{r} \rangle_{\partial\mathcal{T}_h}. \end{aligned}$$

So, since

$$\begin{aligned} \Theta_{\boldsymbol{E}_h} &= (\boldsymbol{H}_h, \nabla \times \boldsymbol{v})_{\mathcal{T}_h} + \langle \boldsymbol{n} \times \boldsymbol{H}_h, \boldsymbol{v} \rangle_{\partial\mathcal{T}_h} - (\boldsymbol{J}, \boldsymbol{v})_{\mathcal{T}_h} + \langle \boldsymbol{n} \times \check{\boldsymbol{v}}, \boldsymbol{H}_h - \boldsymbol{J}_\times \rangle_{\partial\mathcal{T}_h} \\ &= (\boldsymbol{H}_h, \nabla \times \boldsymbol{v})_{\mathcal{T}_h} + \langle \boldsymbol{n} \times \widehat{\boldsymbol{H}}_h^{DG}, \boldsymbol{v} \rangle_{\partial\mathcal{T}_h} - (\boldsymbol{J}, \boldsymbol{v})_{\mathcal{T}_h} \\ &\quad + \langle \boldsymbol{n} \times (\boldsymbol{H}_h - \widehat{\boldsymbol{H}}_h^{DG}), \boldsymbol{v} \rangle_{\partial\mathcal{T}_h} + \langle \boldsymbol{n} \times \check{\boldsymbol{v}}, \boldsymbol{H}_h - \boldsymbol{J}_\times \rangle_{\partial\mathcal{T}_h} \\ &= (\boldsymbol{H}_h, \nabla \times \boldsymbol{v})_{\mathcal{T}_h} + \langle \boldsymbol{n} \times \widehat{\boldsymbol{H}}_h^{DG}, \boldsymbol{v} \rangle_{\partial\mathcal{T}_h} - (\boldsymbol{J}, \boldsymbol{v})_{\mathcal{T}_h} + \theta^1_{\boldsymbol{E}_h} + \theta^2_{\boldsymbol{E}_h}, \\ \Theta_{\boldsymbol{H}_h} &= -\,(\boldsymbol{E}_h, \nabla \times \boldsymbol{r})_{\mathcal{T}_h} - \langle \boldsymbol{n} \times \widehat{\boldsymbol{E}}_h^{DG}, \boldsymbol{r} \rangle_{\partial\mathcal{T}_h} + \theta_{\boldsymbol{H}_h}, \end{aligned}$$

where

$$\begin{aligned} \theta^1_{\boldsymbol{E}_h} &:= \ \langle \boldsymbol{n} \times (\boldsymbol{H}_h - \widehat{\boldsymbol{H}}_h^{DG}), \boldsymbol{v} - \check{\boldsymbol{v}} \rangle_{\partial\mathcal{T}_h}, \\ \theta^2_{\boldsymbol{E}_h} &:= \ \langle \boldsymbol{n} \times \check{\boldsymbol{v}}, \widehat{\boldsymbol{H}}_h^{DG} - \boldsymbol{J}_\times \rangle_{\partial\mathcal{T}_h}, \\ \theta_{\boldsymbol{H}_h} &:= -\,\langle \boldsymbol{n} \times (\check{\boldsymbol{E}}_h - \widehat{\boldsymbol{E}}_h^{DG}), \boldsymbol{r} \rangle_{\partial\mathcal{T}_h}, \end{aligned}$$

if these quantities are equal to zero, then the DG method is a Hamiltonian dynamical system.

But, by Lemma Appendix B.1 with $\boldsymbol{a} := \boldsymbol{H}_h - \widehat{\boldsymbol{H}}_h^{DG}$ and $\boldsymbol{b} := \boldsymbol{v} - \check{\boldsymbol{v}}$, we get that

$$\begin{aligned} \theta^1_{\boldsymbol{E}_h} =& \langle [\![\boldsymbol{H}_h]\!], \{\!\!\{\boldsymbol{v}\}\!\!\} - \check{\boldsymbol{v}} \rangle_{\mathcal{F}_h^0} - \langle \{\!\!\{\boldsymbol{H}_h\}\!\!\} - \widehat{\boldsymbol{H}}_h^{DG}, [\![\boldsymbol{v}]\!] \rangle_{\mathcal{F}_h^0} + \langle \boldsymbol{n} \times (\boldsymbol{H}_h - \widehat{\boldsymbol{H}}_h^{DG}), \boldsymbol{v} - \check{\boldsymbol{v}} \rangle_\Gamma \\ =& \langle [\![\boldsymbol{H}_h]\!], -\underline{\boldsymbol{C}}_{12} [\![\boldsymbol{v}]\!] \rangle_{\mathcal{F}_h^0} - \langle -C_{11} [\![\boldsymbol{E}_h]\!] - \underline{\boldsymbol{C}}_{12}^T [\![\boldsymbol{H}_h]\!], [\![\boldsymbol{v}]\!] \rangle_{\mathcal{F}_h^0} \\ &+ \langle \boldsymbol{n} \times (-C_{11}\, \boldsymbol{n} \times (\boldsymbol{E}_h - \boldsymbol{E}_h^{ext})), \boldsymbol{v} - \boldsymbol{v}^{ext} \rangle_\Gamma, \end{aligned}$$

by the definition of the numerical traces $\breve{\boldsymbol{v}}$, $\widehat{\boldsymbol{H}}_h^{DG}$ and $\widehat{\boldsymbol{E}}_h^{DG}$. Using the definition of $[\![\cdot]\!]$, we finally get that

$$\theta^1_{\boldsymbol{E}_h} = \langle C_{11} [\![\boldsymbol{E}_h]\!], [\![\boldsymbol{v}]\!] \rangle_{\mathcal{F}_h}.$$

So, $\theta^1_{\boldsymbol{E}_h} = 0$ when $C_{11} = 0$. If we now apply Lemma Appendix B.1 with $\boldsymbol{a} := \breve{\boldsymbol{v}}$ and $\boldsymbol{b} := \widehat{\boldsymbol{H}}_h - \boldsymbol{J}_\times$, we get that

$$\theta^2_{\boldsymbol{E}_h} = \langle \boldsymbol{n} \times \breve{\boldsymbol{v}}, \widehat{\boldsymbol{H}}_h - \boldsymbol{J}_\times \rangle_\Gamma = 0,$$

since, by definition of $\breve{\boldsymbol{v}}$, $\boldsymbol{n} \times \breve{\boldsymbol{v}} = \boldsymbol{n} \times \boldsymbol{v}^{ext} = \boldsymbol{0}$ on Γ. Finally, applying Lemma Appendix B.1 with $\boldsymbol{a} := -\breve{\boldsymbol{E}}_h + \widehat{\boldsymbol{E}}_h$ and $\boldsymbol{b} := \boldsymbol{r}$, we get that

$$\theta_{\boldsymbol{H}_h} = -\langle -\breve{\boldsymbol{E}}_h + \widehat{\boldsymbol{E}}_h, [\![\boldsymbol{r}]\!] \rangle_{\mathcal{F}_h^0} + \langle \boldsymbol{n} \times (-\breve{\boldsymbol{E}}_h + \widehat{\boldsymbol{E}}_h), \boldsymbol{r} \rangle_\Gamma = \langle C_{22} [\![\boldsymbol{H}_h]\!], [\![\boldsymbol{r}]\!] \rangle_{\mathcal{F}_h^0},$$

by definition of $\breve{\boldsymbol{E}}_h$ and $\widehat{\boldsymbol{E}}_h$. So, $\theta_{\boldsymbol{H}_h}$ is equal to zero when $C_{22} = 0$. This completes the proof.

Appendix C. Proof of Corollary

Proof. Here we only consider the proof for DG method since the proof for the mixed method is similar and simpler.

To prove the conservation of the electric charge, we define the functional $F_{ec} := (\epsilon \boldsymbol{E}_h, \nabla v)_{\mathcal{T}_h}$ and proceed as follows. We have that

$$\begin{aligned} \dot{F}_{ec} = \{F_{ec}, \mathcal{H}_{\mathcal{E},h}\}_{\mathcal{E},h} &= (\nabla v, \nabla \times (\boldsymbol{H}_h - \boldsymbol{J}_\times))_{\mathcal{T}_h} + \langle \boldsymbol{H}_h - \boldsymbol{J}_\times, \boldsymbol{n} \times \breve{\nabla v} \rangle_{\partial \mathcal{T}_h} \\ &= (\nabla v, \nabla \times (\boldsymbol{H}_h - \boldsymbol{J}_\times))_{\mathcal{T}_h} + \langle \boldsymbol{H}_h - \boldsymbol{J}_\times, \boldsymbol{n} \times \nabla v \rangle_{\partial \mathcal{T}_h}, \end{aligned}$$

since $\breve{\nabla v} = \nabla v$ because ∇v lies in $\boldsymbol{H}(\mathrm{curl}, \Omega)$, see [49, Lemma 3]). Integrating by parts, we get

$$\dot{F}_{ec} = (\nabla \times \nabla v, \boldsymbol{H}_h - \boldsymbol{J}_\times)_{\mathcal{T}_h} = 0,$$

which is what we wanted to prove.

Similarly, for prove the conservation of the magnetic charge, we define $F_{mc} := (\mu \boldsymbol{H}_h, \nabla w)_{\mathcal{T}_h}$, and get that

$$\dot{F}_{mc} = \{F_{mc}, \mathcal{H}_{\mathcal{E},h}\}_{\mathcal{E},h} = -(\boldsymbol{E}_h, \nabla \times (\nabla w))_{\mathcal{T}_h} - \langle \nabla w, \boldsymbol{n} \times \breve{\boldsymbol{E}}_h \rangle_{\partial \mathcal{T}_h}.$$

The first term is obviously zero. To deal with the second term, we apply Lemma Appendix B.1 with $\boldsymbol{a} := \breve{\boldsymbol{E}}_h$ and $\boldsymbol{b} := \nabla w$ to get that

$$\begin{aligned} \dot{F}_{mc} &= -\langle \boldsymbol{n} \times \breve{\boldsymbol{E}}_h, \nabla w \rangle_{\partial \mathcal{T}_h} \\ &= -\langle [\![\breve{\boldsymbol{E}}_h]\!], \{\!\{\nabla w\}\!\} \rangle_{\mathcal{F}_h^0} + \langle \{\!\{\breve{\boldsymbol{E}}_h\}\!\}, [\![\nabla w]\!] \rangle_{\mathcal{F}_h^0} - \langle \boldsymbol{n} \times \breve{\boldsymbol{E}}_h, \nabla w \rangle_\Gamma. \end{aligned}$$

The first term vanishes by the single-valuedness of $\breve{\boldsymbol{E}}_h$ on $\mathcal{F}_h^0$. The second term vanishes by the single-valuedness of $(\nabla w)^t$ on $\mathcal{F}_h^0$, which holds since $\nabla w \in \mathbf{H}(\mathrm{curl}; \Omega)$ and ∇w is a piecewise smooth field (again by [49, Lemma 3]). Finally, since $w = 0$ on Γ, we have $\boldsymbol{n} \times \nabla w = 0$ on Γ. So the third term vanishes as well.

Finally, the energy conservation is a natural consequence of the anti-symmetry of the Poisson bracket. This completes the proof.

Appendix D. Proof of Lemma Appendix B.1

Let the face $F \in \mathcal{F}_h^0$ be the intersection of K^+ and K^-, and denote by $\boldsymbol{f}^+$ and $\boldsymbol{f}^-$ as the restriction of $\boldsymbol{f}$ on F from K^+ and K^-, respectively. Then

$$\begin{aligned}\langle \boldsymbol{n} \times \boldsymbol{a}, \boldsymbol{b} \rangle_{\partial\mathcal{T}_h \setminus \Gamma} =& \langle 1, \boldsymbol{n}^+ \times \boldsymbol{a}^+ \cdot \boldsymbol{b}^+ + \boldsymbol{n}^- \times \boldsymbol{a}^- \cdot \boldsymbol{b}^- \rangle_{\mathcal{F}_h^0} \\ =& \langle [\![\boldsymbol{a}]\!], \{\!\{\boldsymbol{b}\}\!\} \rangle_{\mathcal{F}_h^0} - \langle [\![\boldsymbol{b}]\!], \{\!\{\boldsymbol{a}\}\!\} \rangle_{\mathcal{F}_h^0}.\end{aligned}$$

Indeed,

$$\begin{aligned}&\boldsymbol{n}^+ \times \boldsymbol{a}^+ \cdot \boldsymbol{b}^+ + \boldsymbol{n}^- \times \boldsymbol{a}^- \cdot \boldsymbol{b}^- \\ &= \boldsymbol{n}^+ \times \boldsymbol{a}^+ \cdot \left(\{\!\{\boldsymbol{b}\}\!\} + \frac{\boldsymbol{b}^+ - \boldsymbol{b}^-}{2} \right) + \boldsymbol{n}^- \times \boldsymbol{a}^- \cdot \left(\{\!\{\boldsymbol{b}\}\!\} + \frac{\boldsymbol{b}^- - \boldsymbol{b}^+}{2} \right) \\ &= [\![\boldsymbol{a}]\!] \cdot \{\!\{\boldsymbol{b}\}\!\} + \boldsymbol{n}^+ \times \boldsymbol{a}^+ \cdot \frac{\boldsymbol{b}^+ - \boldsymbol{b}^-}{2} + \boldsymbol{n}^- \times \boldsymbol{a}^- \cdot \frac{\boldsymbol{b}^- - \boldsymbol{b}^+}{2} \\ &= [\![\boldsymbol{a}]\!] \cdot \{\!\{\boldsymbol{b}\}\!\} + (\boldsymbol{b}^+ \times \boldsymbol{n}^+ + \boldsymbol{b}^- \times \boldsymbol{n}^-) \cdot \left(\frac{\boldsymbol{a}^+}{2} + \frac{\boldsymbol{a}^-}{2} \right) = [\![\boldsymbol{a}]\!] \cdot \{\!\{\boldsymbol{b}\}\!\} - [\![\boldsymbol{b}]\!] \cdot \{\!\{\boldsymbol{a}\}\!\}.\end{aligned}$$

This completes the proof.

Appendix E. Proof of Proposition 4.1

Let us prove Proposition 4.1. For the mixed method, we can take $\widehat{\boldsymbol{H}}_h = \boldsymbol{H}_h$ since $\boldsymbol{H}_h \in \mathbf{H}(\mathrm{curl}, \Omega)$. As a consequence, $S_h^M(\boldsymbol{A}_h, \boldsymbol{H}_h) = 0$.

For the HDG method, we obtain the result by simply using the expression of the numerical trace $\widehat{\boldsymbol{H}}_h$ in Table 4, and then recalling that $\boldsymbol{P_M}$ is the $\boldsymbol{L}^2(\partial\mathcal{T}_h)$-projection into $\boldsymbol{M}_h$.

For the DG method, we proceed as follows. By Lemma Appendix B.1 with $\boldsymbol{a} := \widehat{\boldsymbol{H}}_h - \boldsymbol{H}_h$ and $\boldsymbol{b} := \boldsymbol{A}_h - \widehat{\boldsymbol{A}}_h$, we have that

$$\begin{aligned}S_h^{DG}(\boldsymbol{A}_h, \boldsymbol{H}_h) =& - \langle [\![\boldsymbol{H}_h]\!], \{\!\{\boldsymbol{A}_h\}\!\} - \widehat{\boldsymbol{A}}_h \rangle_{\mathcal{F}_h^0} - \langle \widehat{\boldsymbol{H}}_h - \{\!\{\boldsymbol{H}_h\}\!\}, [\![\boldsymbol{A}_h]\!] \rangle_{\mathcal{F}_h^0} \\ &+ \langle \boldsymbol{n} \times (\widehat{\boldsymbol{H}}_h - \boldsymbol{H}_h), \boldsymbol{A}_h - \widehat{\boldsymbol{A}}_h \rangle_\Gamma \\ =& + \langle [\![\boldsymbol{H}_h]\!], \underline{\boldsymbol{C}}_{12} [\![\boldsymbol{A}_h]\!] + C_{22} [\![\boldsymbol{H}_h]\!] \rangle_{\mathcal{F}_h^0} \\ &+ \langle C_{11} [\![\boldsymbol{A}_h]\!] - \underline{\boldsymbol{C}}_{12}^\top [\![\boldsymbol{H}_h]\!], [\![\boldsymbol{A}_h]\!] \rangle_{\mathcal{F}_h^0} \\ &+ \langle \boldsymbol{n} \times (-C_{11}\, \boldsymbol{n} \times (\boldsymbol{A}_h - \widehat{\boldsymbol{A}}_h), \boldsymbol{A}_h - \widehat{\boldsymbol{A}}_h \rangle_\Gamma \\ =& \langle C_{11}\, [\![\boldsymbol{A}_h]\!], [\![\boldsymbol{A}_h]\!] \rangle_{\mathcal{F}_h} + \langle C_{22}\, [\![\boldsymbol{H}_h]\!], [\![\boldsymbol{H}_h]\!] \rangle_{\mathcal{F}_h^0},\end{aligned}$$

by definition of the numerical trace $\widehat{\boldsymbol{H}}_h$, the definition of $[\![\cdot]\!]$, and that of the exterior trace of $\boldsymbol{A}_h$. This completes the proof of Proposition 4.1.

Appendix F. Proof of Lemma 4.1

We want to prove that

$$\langle \boldsymbol{n} \times (\delta \widehat{\boldsymbol{H}}_h^* - \delta \boldsymbol{H}_h), \boldsymbol{A}_h - \widehat{\boldsymbol{A}}_h^* \rangle_{\partial\mathcal{T}_h} = \langle \boldsymbol{n} \times (\widehat{\boldsymbol{H}}_h^* - \boldsymbol{H}_h), \delta \boldsymbol{A}_h - \delta \widehat{\boldsymbol{A}}_h^* \rangle_{\partial\mathcal{T}_h}.$$

For the mixed method, we simply take $\widehat{\boldsymbol{H}}_h := \boldsymbol{H}_h$ (since $\boldsymbol{H}_h \in \mathbf{H}(\mathrm{curl}, \Omega)$) to see that the above equality is trivially satisfied.

For the HDG method, a glance to the definition of the numerical traces $\widehat{\boldsymbol{A}}_h$ and $\widehat{\boldsymbol{H}}_h$ on Table 4, is enough to convince us that the identity is true for this method.

For the DG method, we proceed as follows. By Lemma Appendix B.1 with $\boldsymbol{a} := \delta\widehat{\boldsymbol{H}}_h - \delta\boldsymbol{H}_h$ and $\boldsymbol{b} := \boldsymbol{A}_h - \widehat{\boldsymbol{A}}_h$, we have that

$$
\begin{aligned}
\Phi_h := &\langle \boldsymbol{n} \times (\delta\widehat{\boldsymbol{H}}_h^* - \delta\boldsymbol{H}_h), \boldsymbol{A}_h - \widehat{\boldsymbol{A}}_h^* \rangle_{\partial\mathcal{T}_h} \\
= &-\langle [\![\delta\boldsymbol{H}_h]\!], \{\!\{\boldsymbol{A}_h\}\!\} - \widehat{\boldsymbol{A}}_h^* \rangle_{\partial\mathcal{T}_h} - \langle \delta\widehat{\boldsymbol{H}}_h^* - \{\!\{\delta\boldsymbol{H}_h\}\!\}, [\![\boldsymbol{A}_h]\!] \rangle_{\partial\mathcal{T}_h} \\
&+ \langle \boldsymbol{n} \times (\delta\widehat{\boldsymbol{H}}_h^* - \delta\boldsymbol{H}_h), \boldsymbol{A}_h - \widehat{\boldsymbol{A}}_h^* \rangle_{\Gamma} \\
= &\langle [\![\delta\boldsymbol{H}_h]\!], \underline{\boldsymbol{C}}_{12}[\![\boldsymbol{A}_h]\!] + C_{22}[\![\boldsymbol{H}_h]\!] \rangle_{\mathcal{F}_h^0} + \langle C_{11}[\![\delta\boldsymbol{A}_h]\!] - \underline{\boldsymbol{C}}_{12}^\top[\![\delta\boldsymbol{H}_h]\!], [\![\boldsymbol{A}_h]\!] \rangle_{\mathcal{F}_h^0} \\
&+ \langle \boldsymbol{n} \times (-C_{11}\, \boldsymbol{n} \times (\delta\boldsymbol{A}_h - \delta\widehat{\boldsymbol{A}}_h^*), \boldsymbol{A}_h - \widehat{\boldsymbol{A}}_h^* \rangle_{\Gamma} \\
= &\langle C_{11}\, [\![\delta\boldsymbol{A}_h]\!], [\![\boldsymbol{A}_h]\!] \rangle_{\mathcal{F}_h} + \langle C_{22}\, [\![\delta\boldsymbol{H}_h]\!], [\![\boldsymbol{H}_h]\!] \rangle_{\mathcal{F}_h^0},
\end{aligned}
$$

by definition of the numerical traces $\widehat{\boldsymbol{A}}_h$ and $\widehat{\boldsymbol{H}}_h$, the definition of $[\![\cdot]\!]$, and that of the exterior trace of $\delta\boldsymbol{A}_h$.

On the other hand, By Lemma Appendix B.1 with $\boldsymbol{a} := \widehat{\boldsymbol{H}}_h - \boldsymbol{H}_h$ and $\boldsymbol{b} := \delta\boldsymbol{A}_h - \delta\widehat{\boldsymbol{A}}_h$, we have that

$$
\begin{aligned}
\Psi_h := &\langle \boldsymbol{n} \times (\widehat{\boldsymbol{H}}_h^* - \boldsymbol{H}_h), \delta\boldsymbol{A}_h - \delta\widehat{\boldsymbol{A}}_h^* \rangle_{\partial\mathcal{T}_h} \\
= &-\langle [\![\boldsymbol{H}_h]\!], \{\!\{\delta\boldsymbol{A}_h\}\!\} - \delta\widehat{\boldsymbol{A}}_h^* \rangle_{\partial\mathcal{T}_h} - \langle \widehat{\boldsymbol{H}}_h^* - \{\!\{\boldsymbol{H}_h\}\!\}, [\![\boldsymbol{\delta} A_h]\!] \rangle_{\partial\mathcal{T}_h} \\
&+ \langle \boldsymbol{n} \times (\widehat{\boldsymbol{H}}_h^* - \boldsymbol{H}_h), \delta\boldsymbol{A}_h - \delta\widehat{\boldsymbol{A}}_h^* \rangle_{\Gamma} \\
= &\langle [\![\boldsymbol{H}_h]\!], \underline{\boldsymbol{C}}_{12}[\![\delta\boldsymbol{A}_h]\!] + C_{22}[\![\delta\boldsymbol{H}_h]\!] \rangle_{\mathcal{F}_h^0} + \langle C_{11}[\![\boldsymbol{A}_h]\!] - \underline{\boldsymbol{C}}_{12}^\top[\![\boldsymbol{H}_h]\!], [\![\delta\boldsymbol{A}_h]\!] \rangle_{\mathcal{F}_h^0} \\
&+ \langle \boldsymbol{n} \times (-C_{11}\, \boldsymbol{n} \times (\boldsymbol{A}_h - \widehat{\boldsymbol{A}}_h^*), \delta\boldsymbol{A}_h - \delta\widehat{\boldsymbol{A}}_h^* \rangle_{\Gamma} \\
= &\langle C_{11}\, [\![\boldsymbol{A}_h]\!], [\![\delta\boldsymbol{A}_h]\!] \rangle_{\mathcal{F}_h} + \langle C_{22}\, [\![\boldsymbol{H}_h]\!], [\![\delta\boldsymbol{H}_h]\!] \rangle_{\mathcal{F}_h^0},
\end{aligned}
$$

by definition of the numerical trace $\widehat{\boldsymbol{A}}_h$ and $\widehat{\boldsymbol{H}}_h$, the definition of $[\![\cdot]\!]$, and that of the exterior trace of $\boldsymbol{A}_h$.

This implies that $\Phi_h = \Psi_h$ and completes the proof of Lemma 4.1.

Appendix G. Symplectic integrators

Appendix G.1. Explicit Partitioned Runge-Kutta methods

In Table G.10, we display the coefficients of the Explicit Symplectic Partitioned Runge-Kutta schemes, of s-stages and p-order, ESPRK(s, p), used in our computations. In the section of numerical experiments, we refer to them simply by ESPRK(p).

$$
\begin{array}{cccc|c}
b_1 & 0 & \dots & 0 & b_1 \\
b_1 & b_2 & \ddots & \vdots & b_1 + b_2 \\
\vdots & \vdots & \ddots & 0 & \vdots \\
b_1 & b_2 & \dots & b_s & \sum_{i=1}^{s} b_i \\
\hline
b_1 & b_2 & \dots & b_s &
\end{array}
\qquad
\begin{array}{ccccc|c}
0 & 0 & \dots & & 0 & 0 \\
\tilde{b}_1 & 0 & \ddots & & \vdots & \tilde{b}_1 \\
\tilde{b}_1 & \tilde{b}_2 & \ddots & & & \tilde{b}_1 + \tilde{b}_2 \\
\vdots & \vdots & \ddots & 0 & 0 & \vdots \\
\tilde{b}_1 & \tilde{b}_2 & \dots & \tilde{b}_{s-1} & 0 & \sum_{i=1}^{s-1} \tilde{b}_i \\
\hline
\tilde{b}_1 & \tilde{b}_2 & \dots & \tilde{b}_{s-1} & \tilde{b}_s &
\end{array}
$$

Table G.9: Butcher tableaux of s-stages partitioned Runge-Kutta methods

i	b_i	$\tilde{b}_i$
1	7/24	2/3
2	3/4	−2/3
3	−1/24	1

i	b_i	$\tilde{b}_i$
1	7/48	1/3
2	3/8	−1/3
3	−1/48	1
4	−1/48	−1/3
5	3/8	1/3
6	7/48	0

i	b_i	$\tilde{b}_i$
1	0.1193900292875672758	0.3398396258391100000
2	0.6989273703824752308	-0.0886013369030273329
3	-0.1713123582716007754	0.5858564768259621188
4	0.4012695022513534480	-0.6030393565364911888
5	0.0107050818482359840	0.3235807965546976394
6	-0.0589796254980311632	0.4423637942197494587

Table G.10: Coefficients of the schemes ESPRK(q, p) schemes. From left to right: ESPRK(3,3) [55], ESPRK(6,4) [28], and ESPRK(6,5) [42].

References

[1] N. Anderson and A.M. Arthurs. Helicity and variational principles for Maxwell's equations. International Journal of Electronics, 54(6):861–864, 1983.

[2] S. Blanes and P. C. Moan. Practical symplectic Partitioned Runge-Kutta and Runge-Kutta-Nyström methods. J. Comput. Appl. Math., 142(2):313–330, 2002.

[3] A. Bonito and J.-L. Guermond. Approximation of the eigenvalue problem for the time harmonic Maxwell system by continuous Lagrange finite elements. Math. Comp., 80(276):1887–1910, 2011.

[4] A. Bonito, J.-L. Guermond, and F. Luddens. Regularity of the Maxwell equations in heterogeneous media and Lipschitz domains. J. Math. Anal. Appl., 408(2):498–512, 2013.

[5] S.C. Brenner, F. Li, and L.-Y. Sung. A locally divergence-free interior

penalty method for two-dimensional curl-curl problems. SIAM J. Numer. Anal., 46(3):1190–1211, 2008.

[6] F. Brezzi, J. Douglas, Jr., and L. D. Marini. Two families of mixed finite elements for second order elliptic problems. Numer. Math., 47(2):217–235, 1985.

[7] J.T. Bridges and S. Reich. Numerical methods for Hamiltonian PDEs. J. Phys. A, 39:5287–5320, 2006.

[8] L. Camargo, B. López-Rodríguez, M. Osorio, and M. Solano. An HDG method for Maxwell's equations in heterogeneous media. Comput. Methods Appl. Mech. Engrg., 368:113178, 18, 2020.

[9] R.P. Cameron, S.M. Barnett, and A.M. Yao. Optical helicity, optical spin and related quantities in electromagnetic theory. New Journal of Physics, 14, 2012. 053050.

[10] G. Chen, J. Cui, and L. Xu. Analysis of a hybridizable discontinuous Galerkin method for the Maxwell operator. ESAIM Math. Model. Numer. Anal., 53(1):301–324, 2019.

[11] H. Chen, W. Qiu, and K. Shi. A priori and computable a posteriori error estimates for an HDG method for the coercive Maxwell equations. Comput. Methods Appl. Mech. Engrg., 333:287–310, 2018.

[12] H. Chen, W. Qiu, K. Shi, and M. Solano. A superconvergent HDG method for the Maxwell equations. J. Sci. Comput., 70(3):1010–1029, 2017.

[13] M.-H. Chen, B. Cockburn, and F. Reitich. High-order RKDG methods for computational electromagnetics. J. Sci. Comput., 22/23:205–226, 2005.

[14] W. Chen, Z. Ji, and D. Liang. Energy-conserved splitting finite-difference time-domain methods for Maxwell's equations in three dimensions. SIAM J. Numer. Anal., 48(4):1530–1554, 2010.

[15] Al. Christophe, S. Descombes, and S. Lanteri. An implicit hybridized discontinuous Galerkin method for the 3D time-domain Maxwell equations. Appl. Math. Comput., 319:395–408, 2018.

[16] B. Cockburn and G. Fu. A systematic construction of finite element commuting exact sequences. SIAM J. Numer. Anal., 55(4):1650–1688, 2017.

[17] B. Cockburn, G. Fu, and F.J. Sayas. Superconvergence by M-decompositions. Part I: General theory for HDG methods for diffusion. Math. Comp., 86(306):1609–1641, 2017.

[18] B. Cockburn, Z. Fu, A. Hungria, L. Ji, M.A. Sánchez, and F.-J. Sayas. Stormer-Numerov hdg methods for acoustic waves. Journal of Scientific Computing, 75(2):597–624, 2018.

[19] B. Cockburn and J. Gopalakrishnan. Incompressible finite elements via hybridization. II. The Stokes system in three space dimensions. SIAM J. Numer. Anal., 43(4):1651–1672, 2005.

[20] B. Cockburn, F. Li, and C.-W. Shu. Locally divergence-free discontinuous Galerkin methods for the Maxwell equations. J. Comput. Phys., 194(2):588–610, 2004.

[21] B. Cockburn and C.-W. Shu. The Runge-Kutta discontinuous Galerkin finite element method for conservation laws V: Multidimensional systems. J. Comput. Phys., 141:199–224, 1998.

[22] B. Cockburn and C.-W. Shu. Runge-Kutta discontinuous Galerkin methods for convection-dominated problems. J. Sci. Comput., 16:173–261, 2001.

[23] S. Du and F.-J. Sayas. A unified error analysis of hybridizable discontinuous Galerkin methods for the static Maxwell equations. SIAM J. Numer. Anal., 58(2):1367–1391, 2020.

[24] R. Falk and G.R. Richter. Explicit finite element methods for symmetric hyperbolic equations. SIAM J. Numer. Anal., 36(3):935–952, 1999.

[25] X. Feng and H. Wu. An absolutely stable discontinuous Galerkin method for the indefinite time-harmonic Maxwell equations with large wave number. SIAM J. Numer. Anal., 52(5):2356–2380, 2014.

[26] G. Fu and C.-W. Shu. Optimal energy-conserving discontinuous Galerkin methods for linear symmetric hyperbolic systems. J. Comput. Phys, 394:329–363, 2019.

[27] G.N. Gatica and S. Meddahi. Finite element analysis of a time harmonic Maxwell problem with an impedance boundary condition. IMA J. Numer. Anal., 32(2):534–552, 2012.

[28] E. Hairer, S. P. Nørsett, and G. Wanner. Solving Ordinary Differential Equations I (2Nd Revised. Ed.): Nonstiff Problems. Springer-Verlag New York, Inc., New York, NY, USA, 1993.

[29] J. S. Hesthaven and T. Warburton. High-order nodal discontinuous Galerkin methods for the Maxwell eigenvalue problem. Philos. Trans. R. Soc. Lond. Ser. A Math. Phys. Eng. Sci., 362(1816):493–524, 2004.

[30] J.S. Hesthaven and T. Warburton. Nodal high-order methods on unstructured grids. I. Time-domain solution of Maxwell's equations. J. Comput. Phys., 181:186–221, 2002.

[31] R. Hiptmair. Finite elements in computational electromagnetism. Acta Numer., 11:237–339, 2002.

[32] T. Hirono, W. Lui, S. Seki, and Y. Yoshikuni. A three-dimensional fourth-order finite-difference time-domain scheme using a symplectic integrator propagator. IEEE Trans. Microwave Theory Tech., 49:1640–1648, 2001.

[33] J. Hong and L. Ji. Energy evolution of multi-symplectic methods for Maxwell equations with perfectly matched layer boundary. J. Math. Anal. Appl., 439(1):256–270, 2016.

[34] P. Houston, I. Perugia, and D. Schötzau. Mixed discontinuous Galerkin approximation of the Maxwell operator. SIAM J. Numer. Anal., 42(1):434–459, 2004.

[35] C. Lehrenfeld. Hybrid discontinuous Galerkin methods for solving incompressible flow problems. Rheinisch-Westfalischen Technischen Hochschule Aachen, 2010.

[36] C. Lehrenfeld and J. Schöberl. High order exactly divergence-free hybrid discontinuous Galerkin methods for unsteady incompressible flows. Comput. Methods Appl. Mech. Engrg., 307:339–361, 2016.

[37] L. Li, S. Lanteri, and R. Perrussel. A class of locally well-posed hybridizable discontinuous Galerkin methods for the solution of time-harmonic Maxwell's equations. Comput. Phys. Commun., 192:23–31, 2015.

[38] D.M. Lipkin. Existence of a new conservation law in electromagnetic theory. Journal of Mathematical Physics, 5:695–700, 1964.

[39] P. Lu, H. Chen, and W. Qiu. An absolutely stable *hp*-HDG method for the time-harmonic Maxwell equations with high wave number. Math. Comp., 86(306):1553–1577, 2017.

[40] Ch.G. Makridakis and P. Monk. Time-discrete finite element schemes for Maxwell's equations. RAIRO Modél. Math. Anal. Numér., 29(2):171–197, 1995.

[41] R. McLachlan. Symplectic integration of Hamiltonian wave equations. Numer. Math., 66:465–492, 1994.

[42] R.I. McLachlan and P. Atela. The accuracy of symplectic integrators. Nonlinearity, 5(2):541–562, 1992.

[43] P. Monk. A mixed method for approximating Maxwell's equations. SIAM J. Numer. Anal., 28(6):1610–1634, 1991.

[44] P. Monk. Analysis of a finite element method for Maxwell's equations. SIAM journal on numerical analysis, 29(3):714–729, 1992.

[45] P. Monk. A finite element method for approximating the time-harmonic Maxwell equations. Numer. Math., 63(2):243–261, 1992.

[46] P. Monk. Finite element methods for Maxwell's equations. Numerical Mathematics and Scientific Computation. Oxford University Press, New York, 2003.

[47] P. Monk and G.R. Richter. A discontinuous Galerkin method for linear symmetric hyperbolic systems in inhomogeneous media. Journal of Scientific Computing, 22 and 23:443–477, 2003.

[48] J.-C. Nédélec. Mixed finite elements in $\mathbf{R}^3$. Numer. Math., 35(3):315–341, 1980.

[49] J.-C. Nédélec. A new family of mixed finite elements in $\mathbf{R}^3$. Numer. Math., 50(1):57–81, 1986.

[50] N.C. Nguyen, J. Peraire, and B. Cockburn. Hybridizable discontinuous Galerkin methods for the time-harmonic Maxwell's equations. J. Comput. Phys., 230(19):7151–7175, 2011.

[51] I. Oikawa. A hybridized discontinuous Galerkin method with reduced stabilization. J. Sci. Comput., 65(1):327–340, 2015.

[52] I. Perugia and D. Schötzau. The *hp*-local discontinuous Galerkin method for low-frequency time-harmonic Maxwell equations. Math. Comp., 72(243):1179–1214, 2003.

[53] I. Perugia, D. Schötzau, and P. Monk. Stabilized interior penalty methods for the time-harmonic Maxwell equations. Comput. Methods Appl. Mech. Engrg., 191(41-42):4675–4697, 2002.

[54] P.-A. Raviart and J. M. Thomas. A mixed finite element method for 2nd order elliptic problems. In Mathematical aspects of finite element methods (Proc. Conf., Consiglio Naz. delle Ricerche (C.N.R.), Rome, 1975), pages 292–315. Lecture Notes in Math., Vol. 606, 1977.

[55] R.D. Ruth. A canonical integration technique. IEEE Trans. Nucl. Sci, pages 2669–2671, 1983.

[56] M.A. Sánchez, C. Ciuca, N.C. Nguyen, J. Peraire, and B. Cockburn. Symplectic Hamiltonian HDG methods for wave propagation phenomena. J. Comput. Phys., 350:951–973, 2017.

[57] M.A. Sánchez, B. Cockburn, N.-C. Nguyen, and J. Peraire. Symplectic Hamiltonian finite element methods for linear elastodynamics. Computer Methods in Applied Mechanics and Engineering, 381:113843, 2021.

[58] J.M. Sanz-Serna. Symplectic Runge-Kutta and related methods: recent results. Physica D: Nonlinear Phenomena, 60(1-4):293–302, 1992.

[59] J. Schöberl. NETGEN An advancing front 2D/3D-mesh generator based on abstract rules. Computing and visualization in science, 1(1):41–52, 1997.

[60] J. Schöberl. C++ 11 implementation of finite elements in NGSolve. Institute for Analysis and Scientific Computing, Vienna University of Technology, 30, 2014.

[61] Y. Sun and P.S.P. Tse. Symplectic and multisymplectic numerical methods for Maxwell's equations. J. Comput. Phys, 230:2076—2094, 2011.

[62] Y. Tang and A. E. Cohen. Optical chirality and its interaction with matter. Phys. Rev. Lett., 104:163901, 2010.

[63] Y. Xu, J.J.W. van der Vegt, and O. Bokhove. Discontinuous Hamiltonian finite element method for linear hyperbolic systems. J. Sci. Comput., 35:241–265, 2008.

[64] K. Yee. Numerical solution of initial boundary value problems involving Maxwell's equations in isotropic media. IEEE Transactions on Antennas and Propagation, 14:302—307, 1966.

[65] L. Zhong, S. Shu, G. Wittum, and J. Xu. Optimal error estimates for Nédélec edge elements for time-harmonic Maxwell's equations. J. Comput. Math., 27(5):563–572, 2009.